REPORT DOCUMENTATION PAGE

Form Approved OMB NO. 0704-0188

1. REPORT DATE (DD-MM-YYYY)	2. REPORT TYPE	3. DATES COVERED (From - To)
06-05-2014	Final Report	1-Jul-2007 - 30-Jun-2013

4. TITLE AND SUBTITLE
Plasmonic Bowtie Antenna Nanolaser

5a. CONTRACT NUMBER
W911NF-07-1-0314

5b. GRANT NUMBER

5c. PROGRAM ELEMENT NUMBER
7D10AI

6. AUTHORS
Cun-zheng Ning, Shun-Lien Chuang, Peidong Yang, Ming Wu, Connie Chang-Hasnain

5d. PROJECT NUMBER

5e. TASK NUMBER

5f. WORK UNIT NUMBER

7. PERFORMING ORGANIZATION NAMES AND ADDRESSES
University of California - Berkeley
Sponsored Projects Office
2150 Shattuck Avenue, Suite 300
Berkeley, CA 94704 -5940

8. PERFORMING ORGANIZATION REPORT NUMBER

9. SPONSORING/MONITORING AGENCY NAME(S) AND ADDRESS (ES)
U.S. Army Research Office
P.O. Box 12211
Research Triangle Park, NC 27709-2211

10. SPONSOR/MONITOR'S ACRONYM(S)
ARO

11. SPONSOR/MONITOR'S REPORT NUMBER(S)
53042-EL-DRP.27

12. DISTRIBUTION AVAILIBILITY STATEMENT
Approved for Public Release; Distribution Unlimited

13. SUPPLEMENTARY NOTES
The views, opinions and/or findings contained in this report are those of the author(s) and should not contrued as an official Department of the Army position, policy or decision, unless so designated by other documentation.

14. ABSTRACT
The overarching goal of the NACHOS program is to demonstrate semiconductor lasers that have volume sizes no larger than the cubic of the wavelength in vacuum and can operate at room temperature under electrical injection in continuous-wave mode. Our team has successfully achieved this goal using the semiconductor-metal core-shell design. A secondary goal is to achieve an output power of 2 microwatts under the above operating conditions. We have so far achieved 20 microwatts at 260K and the power scaling indicates that this secondary goal is realizable in the next few months, well within the period of no-cost extension. In addition, many other novel device designs and

15. SUBJECT TERMS
Plasmonic, Nanolaser

16. SECURITY CLASSIFICATION OF:			17. LIMITATION OF ABSTRACT	15. NUMBER OF PAGES	19a. NAME OF RESPONSIBLE PERSON
a. REPORT	b. ABSTRACT	c. THIS PAGE			Peidong Yang
UU	UU	UU	UU		19b. TELEPHONE NUMBER 510-643-1545

Report Title

Plasmonic Bowtie Antenna Nanolaser

ABSTRACT

The overarching goal of the NACHOS program is to demonstrate semiconductor lasers that have volume sizes no larger than the cubic of the wavelength in vacuum and can operate at room temperature under electrical injection in continuous-wave mode. Our team has successfully achieved this goal using the semiconductor-metal core-shell design. A secondary goal is to achieve an output power of 2 microwatts under the above operating conditions. We have so far achieved 20 microwatts at 260K and the power scaling indicates that this secondary goal is realizable in the next few months, well within the period of no-cost extension. In addition, many other novel device designs and fabrication approaches have been explored, showing great promises as alternatives to the core-shell design with other appealing features. The overall project consists of several individual tasks with progress detailed in the following pages.

Enter List of papers submitted or published that acknowledge ARO support from the start of the project to the date of this printing. List the papers, including journal references, in the following categories:

(a) Papers published in peer-reviewed journals (N/A for none)

Received		Paper
05/05/2014	26.00	Hanwei Gao, Anthony Fu, Sean C. Andrews, Peidong Yang . Cleaved-Coupled Nanowire Lasers, Proceedings National Academy of Sciences, (01 2013): 865. doi:
05/05/2014	25.00	Chi-Yu NI, Chien-Yao LU, Akira MATSUDAIRA, Shun Lien CHUANG. Metal-Cavity Nanolasers and NanoLEDs, IEICE Transactions on Electronics, (07 2012): 1235. doi: 10.1587/transele.E95.C.1235
08/15/2012	19.00	K. Ding, Z. Liu, L. Yin, M. Hill, M. Marell, P. van Veldhoven, R. Nöetzel, C. Ning. Room-temperature continuous wave lasing in deep-subwavelength metallic cavities under electrical injection, Physical Review B, (01 2012): 41301. doi: 10.1103/PhysRevB.85.041301
08/15/2012	24.00	Shun Lien Chuang, Erik Stock, Dieter Bimberg, Akira Matsudaira, Chien-Yao Lu, Meng Zhang. Cavity-Volume Scaling Law of Quantum-Dot Metal-Cavity Surface-Emitting Microlasers, IEEE Photonics Journal, (08 2012): 1103. doi: 10.1109/JPHOT.2012.2202315
08/15/2012	23.00	Chi-Yu Adrian Ni, Shu-Wei Chang, Shun Lien Chuang, P. James Schuck. Quality Factor of a Nanobowtie Antenna, Journal of Lightwave Technology, (10 2011): 3107. doi: 10.1109/JLT.2011.2164780
08/15/2012	22.00	Chien-Yao Lu, Shun Lien Chuang. A surface-emitting 3D metal-nanocavity laser: proposal and theory, Optics Express, (06 2011): 13225. doi: 10.1364/OE.19.013225
08/15/2012	21.00	C. Z. Ning, Debin Li. All-semiconductor active plasmonic system in mid-infrared wavelengths, Optics Express, (07 2011): 14594. doi: 10.1364/OE.19.014594
08/15/2012	20.00	D. B. Li, C. Z. Ning. Interplay of various loss mechanisms and ultimate size limit of a surface plasmon polariton semiconductor nanolaser, Optics Express, (07 2012): 16348. doi: 10.1364/OE.20.016348
09/25/2011	1.00	Tzy-Rong Lin, Shun Lien Chuang, Shu-Wei Chang. Theory of Plasmonic Fabry-Perot Nanolasers, Optics Express, (06 2010): 15039. doi: 10.1364/OE.18.015039
09/25/2011	2.00	Shu-Wei Chang, Shun Lien Chuang, Chien-Yao Lu, Tim D. Germann, Dieter Bimberg. Metal-cavity surface-emitting microlaser at room temperature, Applied Physics Letters, (06 2010): 3455316. doi: 10.1063/1.3455316
09/25/2011	3.00	Daniel J. Gargas, Michael C. Moore, Adrian Ni, Shu-Wei Chang, Zhaoyu Zhang, Shun-Lien Chuang, Peidong Yang. Whispering Gallery Mode Lasing from Zinc Oxide Hexagonal Nanodisks, ACS Nano, (06 2010): 3270. doi: 10.1021/nn9018174
09/25/2011	4.00	Chien-Yao Lu, Shu-Wei Chang, Shun Lien Chuang, Tim D Germann, Udo W Pohl, Dieter Bimberg. CW substrate-free metal-cavity surface microemitters at 300 K, Semiconductor Science and Technology, (01 2011): 14012. doi: 10.1088/0268-1242/26/1/014012
09/25/2011	5.00	Shun Lien Chuang, Shu-Wei Chang, Chi-Yu Adrian Ni, Daniel J. Gargas, Michael C. Moore, Peidong Yang. Metal-Coated Zinc Oxide Nanocavities, IEEE Journal of Quantum Electronics, (02 2011): 245. doi: 10.1109/JQE.2010.2073680

09/25/2011 6.00 Shu-Wei Chang, Chien-Yao Lu, Shun Lien Chuang, Tim D. Germann, Udo W. Pohl, Dieter Bimberg. Low Thermal Impedance of Substrate-Free Metal Cavity Surface-Emitting Microlasers,
IEEE Photonics Technology Letters, (08 2011): 1031. doi: 10.1109/LPT.2011.2132124

09/25/2011 7.00 Shu-Wei Chang, Chien-Yao Lu, Shun Lien Chuang, Tim D. Germann, Udo W. Pohl, Dieter Bimberg. Theory of Metal-Cavity Surface-Emitting Microlasers and Comparison With Experiment,
IEEE Journal of Selected Topics in Quantum Electronics, (02 2011): 0. doi: 10.1109/JSTQE.2011.2121894

09/25/2011 8.00 Chien-Yao Lu, Shun Lien Chuang, Alex Mutig, Dieter Bimberg. Metal-cavity surface-emitting microlaser with hybrid metal-DBR reflectors,
Optics Letters, (06 2011): 2447. doi: 10.1364/OL.36.002447

09/25/2011 9.00 Kang Ding, Zhicheng Liu, Leijun Yin, Hua Wang, Ruibin Liu, Martin T. Hill, Milan J. H. Marell, Peter J. van Veldhoven, Richard No?tzel, C. Z. Ning. Electrical injection, continuous wave operation of subwavelength-metallic-cavity lasers at 260 K,
Applied Physics Letters, (06 2011): 231108. doi: 10.1063/1.3598961

09/25/2011 10.00 Hua Wang, Minghua Sun, Kang Ding, Martin T. Hill, Cun-Zheng Ning. A Top-down Approach to Fabrication of High Quality Vertical Heterostructure Nanowire Arrays,
Nano Letters, (04 2011): 1646. doi: 10.1021/nl2001132

09/25/2011 11.00 D. B. Li, C. Z. Ning. Peculiar features of confinement factors in a metal-semiconductor waveguide,
Applied Physics Letters, (05 2010): 181109. doi: 10.1063/1.3425896

09/25/2011 12.00 C. Z. Ning. Semiconductor nanolasers,
physica status solidi (b), (03 2010): 774. doi: 10.1002/pssb.200945436

09/25/2011 13.00 Linus C. Chuang, Michael Moewe, Kar Wei Ng, Thai-Truong D. Tran, Shanna Crankshaw, Roger Chen, Wai Son Ko, Connie Chang-Hasnain. GaAs nanoneedles grown on sapphire,
Applied Physics Letters, (03 2011): 123101. doi: 10.1063/1.3567492

09/25/2011 14.00 Roger Chen, Thai-Truong D. Tran, Kar Wei Ng, Wai Son Ko, Linus C. Chuang, Forrest G. Sedgwick, Connie Chang-Hasnain. Nanolasers grown on silicon,
Nature Photonics, (2 2011): 170. doi: 10.1038/nphoton.2010.315

09/25/2011 15.00 Linus C. Chuang, Forrest G. Sedgwick, Roger Chen, Wai Son Ko, Michael Moewe, Kar Wei Ng, Thai-Truong D. Tran, Connie Chang-Hasnain. GaAs-Based Nanoneedle Light Emitting Diode and Avalanche Photodiode Monolithically Integrated on a Silicon Substrate,
Nano Letters, (02 2011): 385. doi: 10.1021/nl102988w

09/25/2011 17.00 Amit M Lakhani, Kyoungsik Yu, Ming C Wu. Lasing in subwavelength semiconductor nanopatches,
Semiconductor Science and Technology, (01 2011): 14013. doi: 10.1088/0268-1242/26/1/014013

09/25/2011 18.00 S. L. Chuang, D. Bimberg. Metal-Cavity Nanolasers,
IEEE Photonics Journal, (04 2011): 288. doi:

09/25/2011 16.00 Kyoungsik Yu, Amit Lakhani, Ming C. Wu. Subwavelength metal-optic semiconductor nanopatch lasers,
Optics Express, (04 2010): 8790. doi: 10.1364/OE.18.008790

TOTAL: 26

Number of Papers published in peer-reviewed journals:

(b) Papers published in non-peer-reviewed journals (N/A for none)

Received Paper

TOTAL:

Number of Papers published in non peer-reviewed journals:

(c) Presentations

Number of Presentations: 0.00

Non Peer-Reviewed Conference Proceeding publications (other than abstracts):

Received Paper

TOTAL:

Number of Non Peer-Reviewed Conference Proceeding publications (other than abstracts):

Peer-Reviewed Conference Proceeding publications (other than abstracts):

Received Paper

TOTAL:

Number of Peer-Reviewed Conference Proceeding publications (other than abstracts):

(d) Manuscripts

Received Paper

TOTAL:

Number of Manuscripts:

Books

Received Paper

TOTAL:

Patents Submitted

Patents Awarded

Awards

Prof. Peidong Yang

2013 Honorary Fellow, Chinese Chemical Society
2013 Honorary Professor, Griffith University
2013 Overseas Expert, Chinese Academy of Science.
2013 Honorary Professor, Jilin University
2013 Honorary Professor, Xiamen University
2013 ACS Inorganic Nanoscience Award
2012 Honorary Professor, Fudan University
2012 R&D 100 Award
2012 Elected as member of American Academy of Arts and Science

Graduate Students

NAME	PERCENT_SUPPORTED	Discipline
Laklani, Amit	0.50	
Lu, Chien Yao	0.50	
Matsudaira, Akira	0.50	
Ni, Chi Yu	0.25	
Chen, Roger	0.30	
Tran, Thai-Truong Du	0.50	
Li, Kun	0.20	
Shanker, Aamod	0.20	
FTE Equivalent:	**2.95**	
Total Number:	**8**	

Names of Post Doctorates

NAME	PERCENT_SUPPORTED
Gao, Hanwei	1.00
Ding, Kang	1.00
Jin, Leijun	1.00
Prawiharjo, Jerry	0.30
Kim, Myungki	0.88
FTE Equivalent:	**4.18**
Total Number:	**5**

Names of Faculty Supported

NAME	PERCENT_SUPPORTED	National Academy Member
Chuang, Shun Lien	0.15	
Ning, Cun-Zheng	0.17	
Wu, Ming C.	0.18	
FTE Equivalent:	**0.50**	
Total Number:	**3**	

Names of Under Graduate students supported

NAME	PERCENT_SUPPORTED	Discipline
Wei, Eric	0.10	
FTE Equivalent:	**0.10**	
Total Number:	**1**	

Student Metrics

This section only applies to graduating undergraduates supported by this agreement in this reporting period

The number of undergraduates funded by this agreement who graduated during this period: 0.00

The number of undergraduates funded by this agreement who graduated during this period with a degree in science, mathematics, engineering, or technology fields:..... 0.00

The number of undergraduates funded by your agreement who graduated during this period and will continue to pursue a graduate or Ph.D. degree in science, mathematics, engineering, or technology fields:..... 0.00

Number of graduating undergraduates who achieved a 3.5 GPA to 4.0 (4.0 max scale):..... 0.00

Number of graduating undergraduates funded by a DoD funded Center of Excellence grant for Education, Research and Engineering:..... 0.00

The number of undergraduates funded by your agreement who graduated during this period and intend to work for the Department of Defense 0.00

The number of undergraduates funded by your agreement who graduated during this period and will receive scholarships or fellowships for further studies in science, mathematics, engineering or technology fields:..... 0.00

Names of Personnel receiving masters degrees

NAME

Total Number:

Names of personnel receiving PHDs

NAME

Total Number:

Names of other research staff

NAME PERCENT_SUPPORTED

FTE Equivalent:
Total Number:

Sub Contractors (DD882)

Inventions (DD882)

Scientific Progress

See Attachment

Technology Transfer

Final Report: Plasmonic Nanolasers

PI: **Peidong Yang (UC Berkeley)**
Co-PIs: Connie Chang-Hasnain (UC Berkeley)
Shun-Lien Chuang (University of Illinois)
Cun-Zheng Ning (Arizona State University)
Ming Wu (UC Berkeley)

Summary: The overarching goal of the NACHOS program is to demonstrate semiconductor lasers that have volume sizes no larger than the cubic of the wavelength in vacuum and can operate at room temperature under electrical injection in continuous-wave mode. Our team has successfully achieved this goal using the semiconductor-metal core-shell design. A secondary goal is to achieve an output power of 2 microwatts under the above operating conditions. We have so far achieved 20 microwatts at 260K and the power scaling indicates that this secondary goal is realizable in the next few months, well within the period of no-cost extension. In addition, many other novel device designs and fabrication approaches have been explored, showing great promises as alternatives to the core-shell design with other appealing features. The overall project consists of several individual tasks with progress detailed in the following pages.

I. Widegap Semiconductor Nanowire Lasers (Peidong Yang)

I.1 Cleaved-Coupled Nanowire Lasers

As lasers are seeing a rapid increase in applications for digitized communication and signal processing, the monochromaticity of the lasing output becomes an important figure of merit. Laser emission at multiple frequencies can lead to both temporal pulse broadening and false signaling because of group velocity dispersion. These problems can be avoided by controlling the laser to oscillate at a single frequency. Single-mode lasing is obtained when the spectral spacing between the modes, the free spectral range, is larger than the bandwidth of the optical gain. Accordingly, because of their relatively broad gain profile (> 10 nm at room temperature), individual semiconductor nanowires lasing at a single optical frequency would need to be as short as a couple of microns. With low reflectivity of the end facets, such short nanowires are inefficient resonators, and may not have a reachable lasing threshold for the limited gain of the materials.

Here we demonstrate spectral manipulation of lasing modes by axially coupling two nanowire cavities through a nanoscale gap. Lasing operation at a single ultraviolet wavelength at room temperature was achieved in cleaved-coupled GaN nanowires with a total length of up to 9 μm. Besides the reduced number of lasing modes, the cleaved-coupled nanowires also operate with a lower threshold gain than that of the individual component nanowires. Good agreement was found between the measured lasing spectra and the predicted spectral modes obtained from simulated optical coupling properties. The correspondence between the theory and the experiment presents design principles for rational control over the lasing modes in cleaved-coupled nanowire lasers.

Cleaved-coupled nanowires were obtained by defining the optical cavities on single-crystalline GaN nanowires using focused ion beam milling (**Figure I.1a**). This fabrication technique provides precise control over two critical parameters for spectral manipulation of the lasing modes: cavity lengths and inter-cavity gap widths (as narrow as 30 nm). While multiple Fabry-Pérot modes are observed in the lasing spectra of the individual nanowires with lengths of 3.86 μm and 5.14 μm (**Figure I.1b**), single-frequency

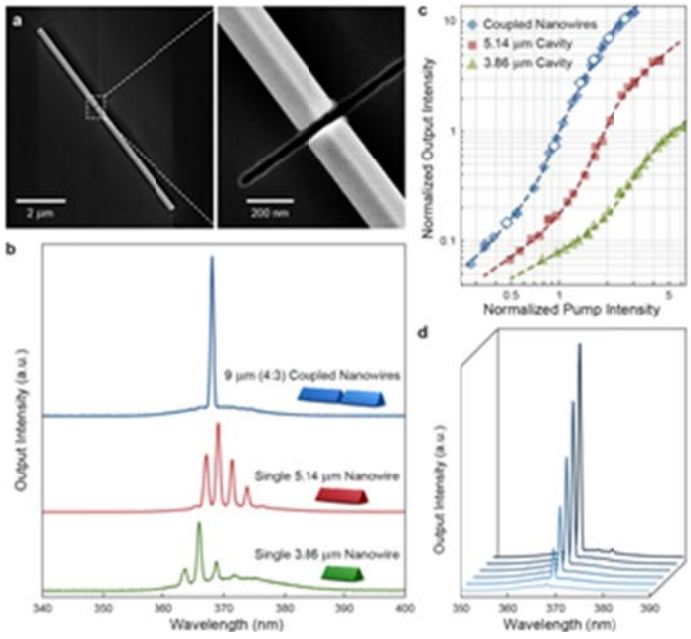

Figure I.1. Single-frequency lasing in 9 μm (4:3) cleaved-coupled nanowires

lasing is generated from the 9 μm (4:3) cleaved-coupled nanowire cavity when the two short cavities are aligned axially with a 40 nm inter-cavity gap. (The notation *x μm (y:z)* describes a cleaved-coupled cavity with a total length of *x μm* and *y:z* is the ratio between the lengths of the two component nanowires.) In addition to the reduced number of lasing modes, the lasing transition occurs at a lower pump power in the cleaved-coupled nanowires (**Figure I.1c**). These two advantages cannot be achieved simultaneously in single Fabry-Pérot nanowire cavities where a larger free spectral range produced in a shorter cavity is always accompanied by a higher threshold gain. The coupled nanowires exhibit stable single-mode operation over a large range of pump energy densities (**Figure I.1d**).

The dimensions of the inter-cavity gaps are found critical to the optical coupling properties in axially coupled nanowires. Finite cross sections of the optical cavity induce severe diffraction losses at the inter-cavity gaps, especially for nanowires with diameters comparable to the effective wavelength. Calculated using three-dimensional full-wave finite-element methods, the transmittance of the nanowire-guided mode through the gap decreases monotonically with an increase in gap width. To maintain effective coupling, the gap width between coupled nanowires needs to be roughly within 30-100 nm where low optical loss and a moderate coupling constant can be obtained. Experimental measurements on cleaved-coupled nanowires with varying gap widths confirmed the predictions from simulations. While 9 μm (4:3) coupled nanowires with a 60-nm gap can produce single-frequency lasing, multimode operation is observed when the gap width was increased to 150 nm.

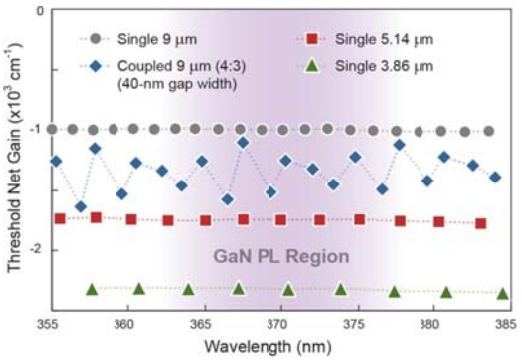

Figure I.2. Lasing modes calculated based on transfer matrix methods.

The spectral modulation of modes observed in cleaved-coupled nanowire lasers can be predicted with good agreement using transfer matrix methods based on the calculated optical properties of the inter-cavity gaps. The calculated eigenvalues for 9 μm (4:3) coupled nanowires with a 60-nm gap show significant modulation of the threshold gain among different lasing modes (**Figure I.2**, blue diamonds). Within the bandwidth of the GaN gain profile, only one mode is outstanding with the lowest threshold gain. In contrast, modes predicted for single nanowires have nearly equal threshold gains and multiple modes are expected in their lasing output. Moreover, for the modes of coupled cavities, both component nanowires provide the optical gain; therefore, the net gain required for coupled nanowires to reach lasing transitions is expected to be lower than that for each individual nanowire (**Figure I.2**, red squares and green triangles), which agrees well with the experimental results (**Figure I.1c**) and confirms the two benefits (i.e. lower threshold and fewer modes) of the coupled nanowire lasers.

The analytical model for mode calculations allows rational design of cleaved-coupled nanowires for the selection of desirable modes. Integer or fractional ratios between the lengths of the component nanowires make a significant difference in the free spectral range of the coupled nanowires. The lasing spectra confirm that 9 μm (1:1) and 9 μm (2:1) coupled nanowires show a modulation in the threshold gain that follows the resonances in the shorter cavities (**Figure I.3**). Alternatively, fractional ratios lead to modulation in the threshold gain at low-frequency spectral periodicities by a beating effect, which is therefore favorable for achieving single-frequency operation in cleaved-coupled nanowire lasers.

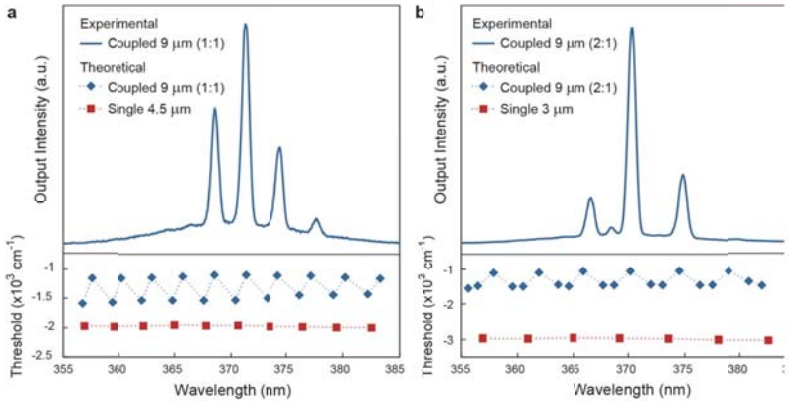

Figure I.3. Measured lasing spectra and calculated modes of cleaved-coupled nanowires with integer ratios between the lengths of the component nanowires.

Our work offers a promising and practical route toward improved quality of lasing from semiconductor nanowires. Along with simple geometric designs and precise fabrication techniques, the excellent agreement between the theoretical predictions and the experimental observations allows reliable and rational control of the lasing modes in nanowires. While single-frequency lasing is demonstrated here in GaN nanowires, the principles for selecting modes using cleaved-coupled nanowire lasers should not be restricted to a specific material, operating wavelength, or pumping scheme. The idea of axial coupling can also be extended to coupled cavities containing more than two nanowires to achieve more complicated modulation of lasing modes. This compact, one-dimensional architecture is highly reproducible and can be suited for integration into chip-based photonic circuits. The highly monochromatic light from coupled nanowire lasers is anticipated to provide ultra-compact photon sources for laser-based remote sensing, optical data storage, and long-distance optical communication.

I.2 P-Type Transport in Li-doped ZnO Nanowires

Due to the wide band gap (3.4 eV) and large binding energy (~60 meV), ZnO is suitable for short wavelength photonic applications, such as ultraviolet lasers, light-emitting diodes, and solar cells. However, such high quality optoelectronic devices rely on reliable of both n- and p-type ZnO. Most ZnO is grown intrinsically n-type, thereby making p-type doping of extreme importance. However, low solubility of dopants, high defect ionization energies, and intrinsic donor defect

compensation, such as Zn interstitials (Zn_i) and O vacancies (V_o), have provided difficulties towards this goal. In this study, Li was chosen as the dopant towards p-type behavior is ZnO. Unlike other larger cation dopants, the relatively small size of Li increases the allowable solubility. Additionally, the donor defect state of the substitution Li (Li_{Zn}) lies ~150 meV from the valence band edge, which is lower than several other metallic dopants.[1]

Figure I.2 ZnO nanowire lasers

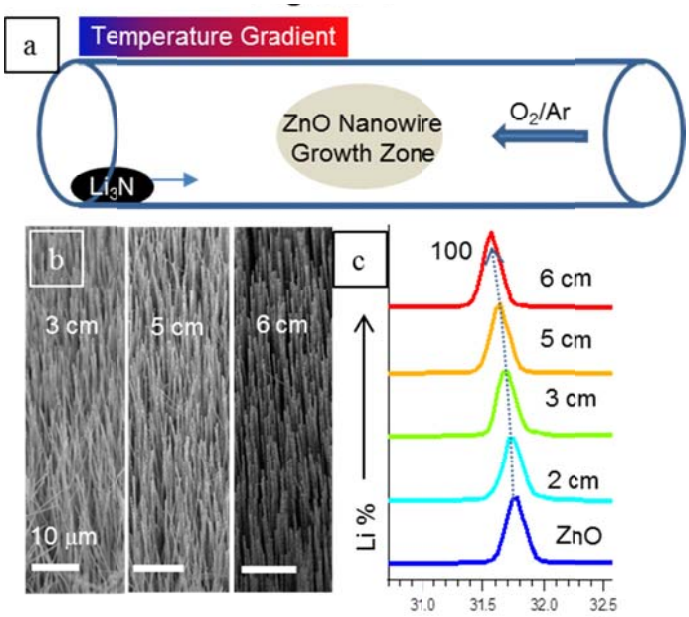

Li-doped ZnO nanowires were synthesized via physical vapor deposition while in the presence of Li_3N (**Figure I.2a**). The amount of Li present in the ZnO growth zone was qualitatively controlled by adjusting the Li_3N position relative to the growth zone: the closer the precursor to the growth zone, the higher the temperature (and vapor pressure), thereby introducing more Li for uptake into the ZnO. This takes advantage of the inherent temperature gradient of the tube furnace while not changing the growth condition of the ZnO nanowires (**Figure I.2b**). Li incorporate into the ZnO nanowires was confirmed by a shift in the ZnO (100) diffraction peak (**Figure I.2c**). Compared with pure ZnO nanowires, lattice expansion is observed as a function of Li_3N position, with the largest *a* parameter occurring at the 6 cm position. This expansion is attributed to the location of the Li dopants[2,3], which predominately exist in the octahedral interstitial site (Li_i) and as a Li_i-Li_{Zn} complex within the wurtzite lattice.[4]

The effect of the *in situ* CVT doping on electrical transport was investigated by single nanowire field-effect transistor and thermopower measurements (**Figure I.3a**). The as-grown Li-doped ZnO nanowires exhibited high resistances but responded n-type, with the average mobility and electron concentration of 5.2 ± 3.2 $cm^2V^{-1}s^{-1}$ and between 10^{15}-10^{16} cm^{-3}, respectively. Seebeck coefficient (S_c) measurements confirmed that electrons were still the majority carrier. Because of the large amount of Li required to shift the lattice parameter (on the order of 2-6%), a decrease of the mobility and increase in the S_c as compared to pure ZnO nanowires was expected. However, considering that Li_i can act as donor, the reduced carrier concentration may be the consequence of the weak acceptor behavior of the Li_{Zn}-Li_i complex.[4]

To break the Li_{Zn}-Li_i bond and aid Li_{Zn} formation, an on-device anneal (500 ^oC, O_2, 1 hour) was performed on the Li-doped ZnO nanowire as a 'dopant activation' step. As seen in **Figure I.3b**, the back-gated response of the device switches from n-type behavior to p-type behavior. The

now p-type ZnO nanowires exhibit both higher mobilities (10.4 $\pm$ 5.4 $cm^2V^{-1}s^{-1}$)and carrier

Figure I.3 p-type ZnO nanowires

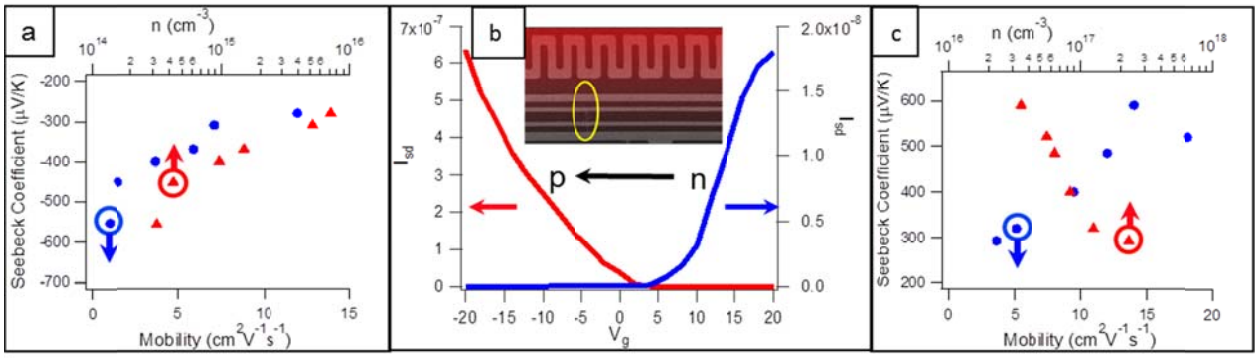

concentrations (~10^{16} - 10^{17} cm^{-3}) then before the annealing. Additionally, the threshold voltage remains positive even after activation. Effectively, the "normally off" n-type channel was converted to a "normally on" p-type channel. The sign of the Seebeck also switches to positive voltages after the annealing step, providing further evidence that holes are the majority carrier (**Figure I.3c**). With further optimization of dopant incorporation and activation, increases in overall conductance can be achieved for optimal optoelectronic device performance.

1. Zeng, Y.J. *et al.* Identification of acceptor states in Li-doped p-type ZnO thin films. *Applied Physics Letters* **89**, 042106 (2006).
2. Lee, J. *et al.* P-type conduction characteristics of lithium-doped ZnO nanowires. *Advanced materials (Deerfield Beach, Fla.)* **23**, 4183-7 (2011).
3. Yi, J.B. *et al.* Ferromagnetism in Dilute Magnetic Semiconductors through Defect Engineering: Li-Doped ZnO. *Physical Review Letters* **104**, 1-4 (2010).
4. Vidya, R., Ravindran, P. & Fjellva, H. Ab-initio studies on Li doping , Li-pairs , and complexes between Li and intrinsic defects in ZnO. **123713**, 1-10 (2012).

II. Semiconductor-Metal Core-Shell Nanolasers and Their Size-Limit (Cun-Zheng Ning)

II.1 Room Temperature Operation with Record Performance

This task adopts the original core-shell approach [1], as was proposed at the beginning of the NACHOS program. Over the course of the program, the design and fabrication have been significantly improved and optimized. Various records have been achieved using this approach, including the first electrical injection lasers with a dimension below the diffraction limit, breaking the half-wavelength limit [2] for the first time. This design allowed the operation of the sub-wavelength laser to operate at a record high temperature at 260 K two years ago [3], and at room temperature recently [4]. One of the key issues with the room temperature operation is the relatively broad linewidth.

By improving the design and fabrication, we have [5,6] finally demonstrated in a more convincing manner a nanolaser under electrical injection with a sub-wavelength cavity volume of $0.67\lambda^3$operating in CW mode at room temperature, thus achieving one of the most important programmatic goals of NACHOS project. A more sophisticated power measurement has been carried out using the integration sphere, indicating the possibility of reaching 2 micron watts total output power. In addition, we studied nanolasers with circular cross section. Azimuthally polarized laser beam from small nanolaser supporting TE_{01} mode is verified experimentally. Room temperature operation is achieved on some larger devices as well. Following are more detailed report describing the specific milestones achieved:

Major Results:

- **Record performance of CW room temperature operation under electrical injection:** Fig. II.1. shows the lasing characteristics of a nanolaser with physical cavity volume of 1.15 (W) × 1.39 (L) × 1.7 (H) $\mu m^3 = 0.67\ \lambda^3$ (λ=1591 nm).

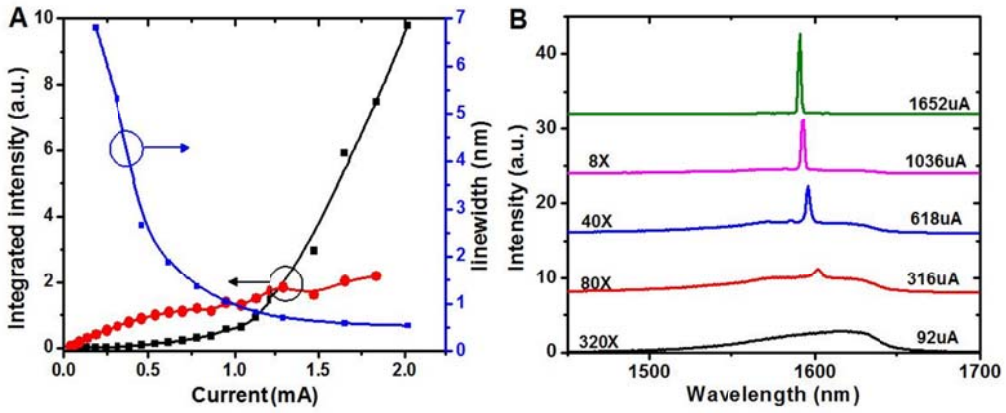

Figure II.1 A: L-I and FWHM-I curve at 294K under DC current injection of the laser. Black squares ■: integrated lasing mode intensity; Red solid circles ●: integrated spontaneous emission intensity. B: Spectra (offset for clarity) of this device at different currents

This device shows a clear threshold current at 1.1 mA. The linewidth drops continuously to 0.5 nm which is 1/6 of our previous room temperature result. Polarization resolved measurement shows the lasing emission is linearly polarized along device length direction, consistent with the FDTD simulation. So far this result is comparable or better than other room temperature pulse sub-wavelength lasers and approaching conventional RT CW semiconductor lasers.

- **Power measurement at high temperature:** We performed power measurements on our sub-wavelength nanolasers at high temperature (>200 K) where the nanolasers show an CW output power on the order of tens of microwatts (see Fig. II.2). At room temperature, the output power is so low that beyond our measurement ability. Even at 260 K, the power of this device can be up to 20 μW. A current efficiency is defined as the slope of power-current curve. The drop of this efficiency represents the degradation of device performance as temperature increases.

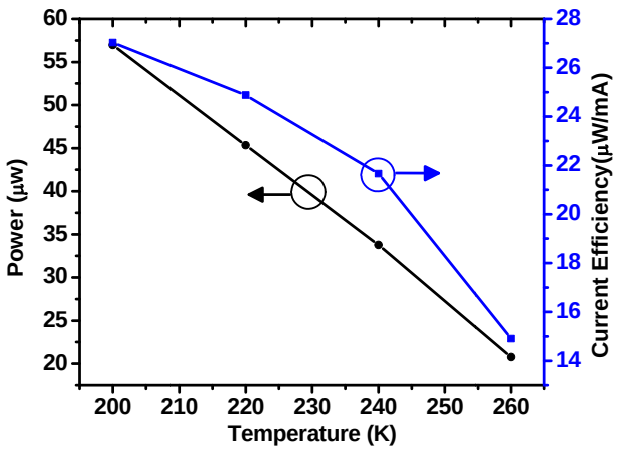

Figure II.2 The output power and current efficiency from a device with cavity volume of 0.88 μm (W) X 1.69 μm (L) X 1.70 μm (H) at DC voltage of 4V and injection current ~2mA. Measurements were conducted from 200 K to 260 K.

II.2 Circular Core-Shell Structure with Azimuthal Polarization

Metallic cavity nanolasers with circular geometry also exhibited interesting polarization properties and can be explored for some interesting applications. Radially or azimuthally polarized laser beams have many interesting applications. But so far, such beams have been generated under optical pumping, using external optics, or fabricating gratings on top of a VCSEL. A compact nanoscale electrically driven laser source with azimuthally polarized beam has not been reported so far. Through our simulation, we found that in small circular nanolasers, single mode operation with specific operation can be achieved. Fig. II.3 shows our FDTD simulation result for small circular nanolasers showing the resonance wavelength dependence on

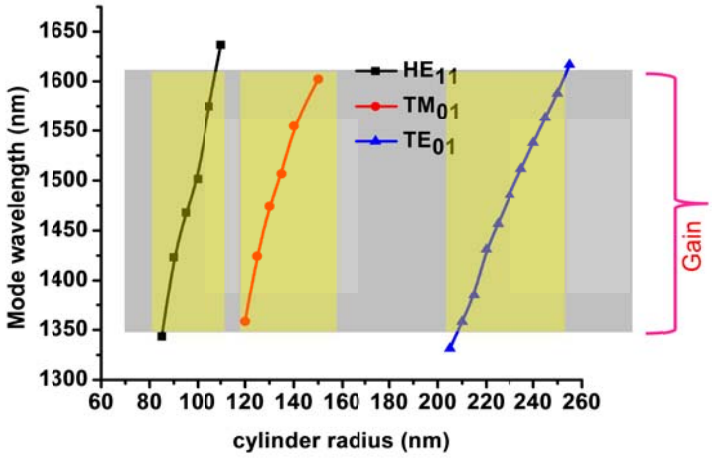

Figure II.3 Resonance wavelengths of the three lowest order modes in a small circular laser with radius from 80 to 260 nm.

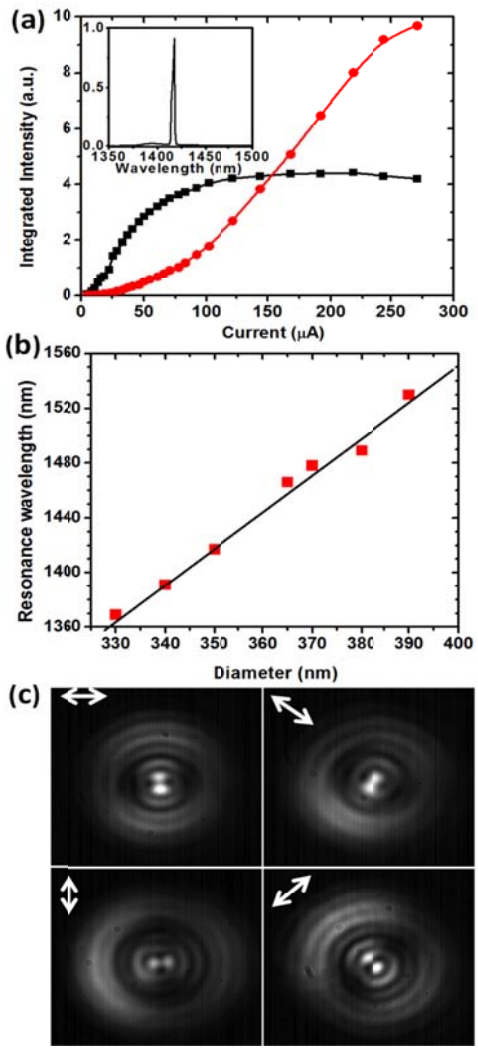

Figure II.4 (a): CW lasing characteristics from a device with total cavity volume of 0.146 λ3. L-I curve shows a threshold current at 80 μA. Inset is the lasing spectrum at 196 μA. (b): Linear shift of resonance wavelength from 1.37 μm to 1.53μm. Shifting slope is 2.7, (c): Laser output images taken by a NIR camera behind a linear polarizer along the direction indicated by the white arrows. The dark line splitting the image along the polarizer direction (white double arrow) confirms the azimuthal polarization of the laser output.

operation. Fig. II.5 shows the room temperature lasing characteristics of a circular nanolaser with radius 700 nm under pulse current injection.

device diameter. The mode spacing of the three lowest modes HE_{11}, TM_{01} and TE_{01} is so large that only one mode will fall within material gain bandwidth, thus enabling controllable selection of a single mode.

CW lasing under electrical injection is achieved on the device with semiconductor core diameter of 350 nm, corresponding to a total cavity volume of 0.146 λ^3. Its lasing characteristics are shown in Fig. II. 4. This device supports TE_{01} mode. The output beam image after passing through a linear polarizer is shown in Fig. II,4(c). The azimuthal polarization predicted in our simulation is verified by the dark line along the polarizer direction in such images.

Circular devices also allow better performance with smaller overall volume. Some circular devices with somewhat larger diameters can achieve room temperature

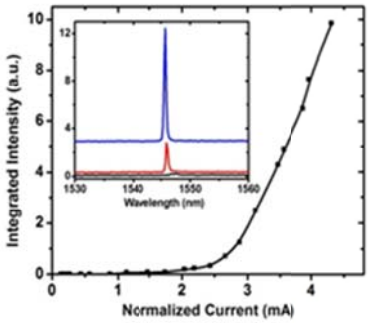

Figure II.5 L-I curve of a device with radius of 700nm at room temperature (296K) under pulse current injection (30ns pulse width/1MHz repetition rate). The current is normalized The inset shows the spectra at different currents of 2.13mA (black), 3.07mA (red) and 3.83mA (blue).

II.3 Theoretical Modeling and Simulation: Ultimate Size Limit of a Plasmonic Nanolaser

During the course of this project, simulation and modeling was an integral part of the project execution and played an important role in predicting and analyzing the ultimate potential of device performance. One of the important results is the possibility of doing plasmonics without metals which are lossy and difficult to produce with high quality. Our analysis shows that InAs heterostructures is the best material choice and can potentially realize plasmon resonance in the near-infrared [10]. Furthermore, such all-semiconductor approach allows ready integration of active and passive components using pure epitaxial growth with minimal loss. Another predication of our modeling is the ultimate size limit of a plasmonic nanolaser [9]. We find that there is an interesting interplay between the facet loss and the SPP propagation loss and that such interplay leads to the existence of a minimum-threshold mode in each mode group. The red-shift of the minimum-threshold mode with the decrease of device thickness leads to a further reduction of threshold gain, making the threshold for the SPP nanolaser achievable for many semiconductors, even at room temperature. In addition, we find that the threshold can be further reduced by using thinner metal cladding without much exacerbated mode leakage. Finally, a specific design example (see Fig. II.6) is optimized using $Al_{0.3}Ga_{0.7}As/GaAs/Al_{0.3}Ga_{0.7}As$ single quantum well sandwiched between silver layers, which has a physical volume of $1.5 \times 10^{-4} \lambda_{30}$, potentially the smallest semiconductor nanolasers designed or demonstrated so far.

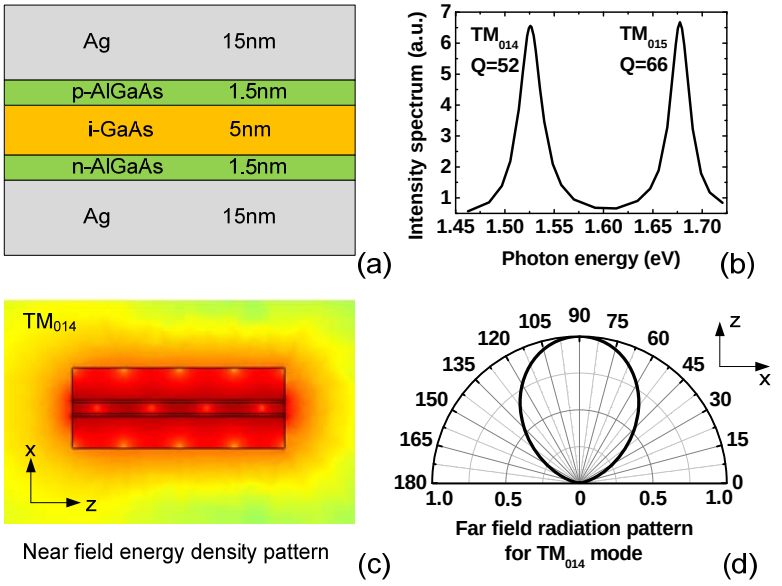

Figure II.6 (a) Schematic structure of an optimized MISIM nanolaser. (b) Intensity spectrum of the nanolaser within the gain bandwidth of AlGaAs/GaAs/AlGaAs quantum well showing two possible modes. (c) Near field energy density pattern of the TM014 mode at lasing threshold in the *x*-*z* plane. (d) Angular dependence of the far field $|E|^2$ radiation pattern of the TM_{014} mode at the lasing threshold in the *z*-*x* plane.

References for Section II

[1] A.V. Maslov and C.Z. Ning, Size reduction of a semiconductor nanowire laser using metal coating", SPIE Proceed. Vol.**6468**, 64680I (2007).

[2] Martin T. Hill, Milan Marell, Eunice S. P. Leong, Barry Smalbrugge, Youcai Zhu, Minghua Sun, Peter J. van Veldhoven, Erik Jan Geluk, Fouad Karouta, Yok-Siang Oei, Richard Nötzel, Cun-Zheng Ning, and Meint K. Smit, Lasing in metal-insulator-metal sub-wavelength plasmonic waveguides, *Optics Express*, Vol. **17**, Issue 13, pp. 11107-11112, 2009.

[3] K. Ding, Z.C. Liu, L.J. Yin, H. Wang, R.B. Liu, M. T. Hill, M. J. H. Marell, P. J. van Veldhoven, R. Nötzel, and C. Z. Ning, Electrical injection, continuous wave operation of subwavelength-metallic cavity lasers at 260 K, *Appl. Phys. Lett.*, **98**, 231108, 2011.

[4] K. Ding, Z.C. Liu, L.J. Yin, M. T. Hill, M. J. H. Marell, P. J. van Veldhoven, R. Nötzel, and C. Z. Ning, Room-temperature continuous wave lasing in deep-subwavelength metallic cavities under electrical injection, *Phys. Rev. B* **85**, 041301(R), 2012.

[5] K. Ding, M. T. Hill, Z.C. Liu, L. J. Yin, D. Sahin, P. J. van Veldhoven, E. J. Geluk, T. D. Vries and C.Z. Ning, Record Performance of a CW Metallic Subwavelength- Cavity Laser at Room Temperature, CLEO/QELS, San Jose, CA, May 7-11, 2012.

[6] K. Ding, Z. Liu, L. Yin, M. T. Hill, J. H. Marell, P. J. Van Veldhoven, R. Noetzel, C. Z. Ning, Demonstration of Electrical Injection Sub-wavelength Metallic-Cavity Semiconductor Lasers at Room Temperature, submitted for publication

[7] K. Ding; Z. Liu; L. Yin; M. T. Hill; J. H. Marell; P. J. Van Veldhoven; R. Noetzel; C. Z. Ning, An Electric driven metallic nanocavity laser generating azimuthally polarized beam, in preparation for publication

[8] K. Ding and C. Z. Ning, Metallic subwavelength-cavity semiconductor nanolaser. (an invited review), Light: Science and Applications, (2012)

[9] D.B. Li, and C.Z. Ning, Interplay of various loss mechanisms and ultimate size limit of a surface Plasmon polariton semiconductor nanolaser, *Opt. Express **20**, 16348, 2012.*

[10] D.B. Li and C.Z. Ning, All-semiconductor active plasmonic system in mid-infrared wavelengths", *Opt. Express*, **19**, 14594, 2011.

III. Metal-Cavity Surface Emitting Nanolaser (Shun-Lien Chuang)

III.1 Development of 980 nm Metal-Cavity Surface-Emitting Micro/NanoLasers

To have a wider application range for metal-cavity lasers, we gradually move the spectra from 850 nm to 1550 nm. During the phase-II project, we have successfully applied our process techniques for 850 nm metal-cavity surface-emitting lasers to longer wavelength lasers (980 nm and 1550 nm). The experiments were initiated with conventional VCSEL samples with 37 DBR pairs and a hybrid mirror (composed of 23 DBR pairs plus silver) as shown in Fig. 1 [1]. Continuous-wave operation at room-temperature was demonstrated for a volume of 12 λ_0^3 at 980 nm with the power increasing to more than 8 μW, compared to our previous work.

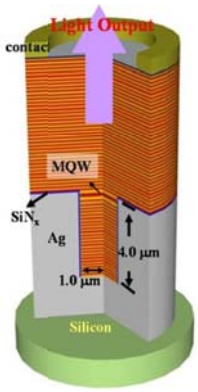

Figure 1. The structure of a 980 nm metal-cavity surface-emitting microlaser. The cavity was formed by a hybrid mirror (23 DBR pairs + Ag) and 37 DBR pairs. Devices worked under CW current injection at room temperature with outputs greater than 8 μW. [1]

We have designed a few 980 nm layered structures with reduced or only one-sided DBR as feedback mirrors. Several combinations are theoretically investigated with reduced volumes. For example, in Fig. III. 2, a design with a total number of 12 DBR pairs is analyzed. The volume is bounded to below 1 λ_0^3 to meet the Phase-III final goal. The analysis shows a promising result for achieving room temperature continuous-wave operation.

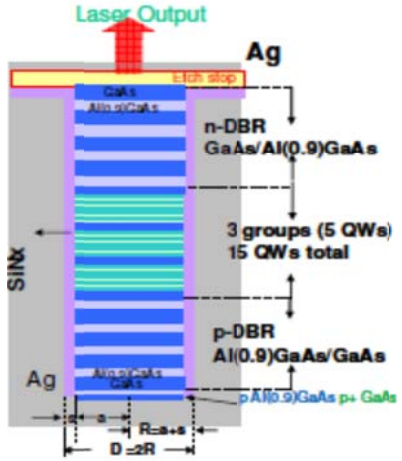

Figure. III. 2. A 12-pair DBR design with 15 multiple quantum wells as active region. The structure is optimized for quantum well positions. The table shows the properties at 300 K, the thresholds are all below 1500 cm^{-1} and should be achievable at room temperature. The smallest design is 0.65 □m in diameter with a cavity volume of 1.0 □$_0^3$.

All @ 300K	2a=0.65um	2a=0.80um	2a=1.20um	2a=2.00um
Diameter (D=2a+2s)	0.77um	0.92um	1.32um	2.12um
Height	2.059um	2.059um	2.059um	2.059um
Volume(lambda^3)	1.00	1.42	2.94	7.60
Lasing wavelength	962nm	972nm	985nm	992nm
Threshold gain	1471cm-1	1359cm-1	1277cm-1	1261cm-1

III.2 NanoLasers and NanoLEDs without DBRs

We have fabricated metal encapsulated nano-cavity light emitting diodes operating with electrical injection at room temperature. The active region of the device is bulk InGaAs with InP as the carrier injector. An etching stop layer of InGaAsP is inserted in between InP and substrate for substrate removal purposes. Figure III.3(a) and 3(b) show the schematics of the device which is flip-chip bonded to silicon substrate wafer. The metal-defined nano disk has a thickness of 200 nm and a radius of about 1 μm. The sidewall of disk is passivated with approximately 100 nm silicon nitride before metallization. This layer serves to passivate the sidewall, provides electrical isolation between the anode and cathode, and is an optical cladding layer between the active disk and metal. Silver is chosen to define the metal cavity for its smaller optical absorption compared

to other metals. The cavity volume encapsulated by silver is ~ 0.76 μm^3, which corresponds to only 0.19 λ_0^3 where λ_0 is the free space emitted wavelength.

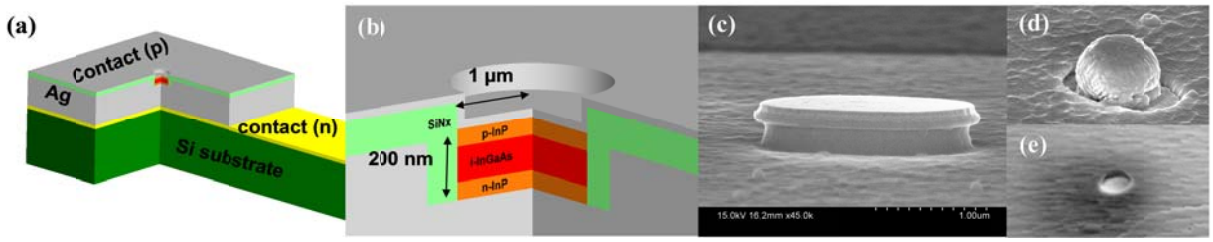

Figure III. 3. (a) Schematic of metal encapsulated nano-cavity light emitter. (b) Detailed structure of active cavity region. SEM images of processed device after (c) thin SiNx passivation on sidewall and floor, (d) thick silver deposition on device top and sidewall, and (e) finished sample viewing from the top. [2]

Scanning electron micrographs (SEM) of critical steps in processing the device are shown in Fig. III. 3(c), 3(d), and 3(e). After the p-i-n junction disk is defined by etching processes, silicon nitride is uniformly covered for passivation and electrical insulation. Then, only the top side of the silicon nitride is selectively removed for electrical injection (Fig. III. 3c). After a thick silver layer is deposited on the top and side (Fig. III. 3d), the device is flip-bonded on a silicon substrate with a gold electrode pad. Figure III.3(e) shows finished sample from the top view after substrate removal and deposition of a thin silver contact layer (40 nm in this work), which serves as the anode contact. By varying the top sliver thickness, it is possible to control the optical confinement factor Q.

Figure III. 4(a) shows cross sectional electrical field simulated by the finite-difference time-domain (FDTD) method. The simulation result shows the fundamental HE_{111} mode with a quality factor Q of 196 at the resonant wavelength. Fig.III. 4(b) shows the voltage vs. current (V-I) and light output vs. current (L-I) curves at two different temperatures. The V-I curve indicates good isolation between the anode and cathode by the thin 100 nm silicon nitride layer, showing a typical diode threshold voltage at 1.06 V. The two L-I curves show a decreasing slope efficiency with increasing temperature. At 15°C and 28 °C, the slope efficiency is 0.31 and 0.27 mW/A respectively. We have successfully overcome the processing challenges of forming an electrical injection device for a metallic nano cavity with a heterojunction thickness of 200 nm. Electroluminescence (EL) spectrums of a processed device and the photoluminescence (PL) spectrum of the epiwafer measured at room temperature (28 °C) are shown in Fig. 4(c). Despite no lasing activity, the EL spectrum from the device shows no degradation during the process compared to pre-processing PL data.

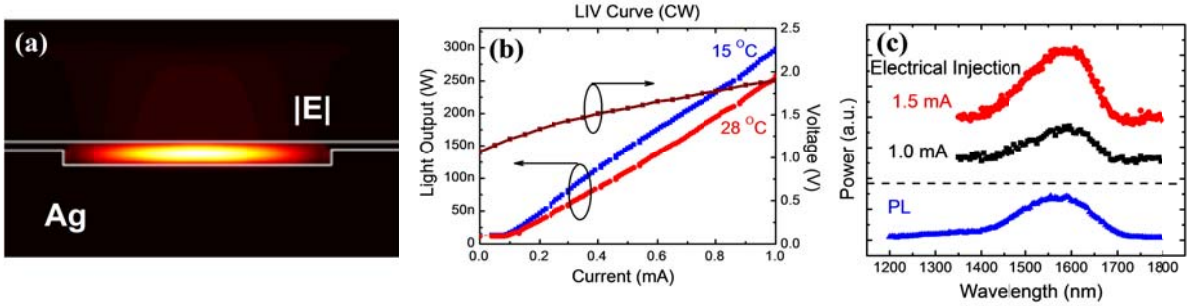

Figure III.4. (a) A cross-sectional FDTD simulated field profile of the device showing the fundamental HE_{111} mode. (b) The light output and voltage vs. current curves showing clear diode turn-on behaviour. (c) Electroluminescence and photoluminescence spectrum at room temperature.

We have also designed a larger cavity volume metal encapsulated device for higher quality factor in an attempt to fabricate a lasing device. Figure III. 5(a) shows the device schematic and FDTD simulation for the fundamental HE_{116} mode for this design. The quality factor of this design is around 700, significantly larger than the previous thin design. Figure III. 5(b) is an electrical injection, CW, optical spectrum at room temperature. The cavity dimensions are; radius = 1 μm, height = 1.599 μm, cavity volume = 1.23 λ_0^3. Even though the cavity volume is larger than the previous device, room temperature spectrum narrowing was observed where the output power increased to slightly over 1 μW.

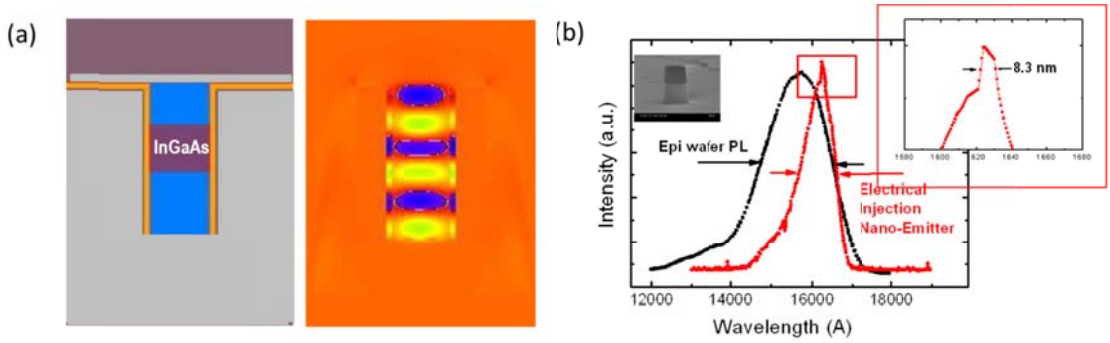

Figure III. 5. (a) Schematic and FDTD simulation for metal-cavity, electrical injection nano emitter with a total p-i-n junction thickness of 1599 nm. (b) Electrical injection optical spectrum compared with epiwafer PL data measured at room temperature showing spectrum narrowing. [2]

III.3 Theory on the design rules and optimization of a nano-coin laser [3]

We have formulated and established the fundamental frame work for the theory of metal-cavity nanolasers [3]. During the last year, we applied our theory to new structure designs such as nano-coin lasers and nanoLEDs. Several design optimizations are proposed and verified by full-structure numerical analyses. To further simplify and generalize the design rule, a Fabry-Perot analogy of nanolaser is summarized and used to design our DBR-free metal-cavity nanolasers. The simplified FP model of the HE11 mode includes all the necessary parameters for the design and predicts the performance with a very good agreement with the full-structure FDTD and FEM methods. Figure 6 shows the calculated result from the FP model of a nano-coin structure with p-InP (40 nm)/i-InGaAs (160 nm)/ n-InP(40 nm). The design agrees very well with the prediction of FDTD. We are making progress toward fabricating the nano-coin lasers.

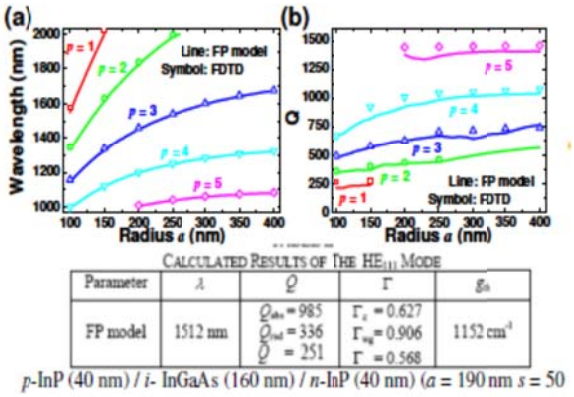

Figure. III. 6. Calculations of a nano-coin laser (*p*-InP:40 nm /*i*-InGaAs:160 nm /*n*-InP:40 nm) (a) resonant wavelength and (b) quality factor as a function of device radius. The table shows calculated properties of the smallest possible cavity HE_{111}. With proper design, a CW room-temperature nanolaser is achievable with reasonable gain and ultrasmall volume 0.02 $\square_0^3$

III.4 Cavity Volume Scaling Law of Quantum-Dot Metal-Cavity Surface-Emitting Microlasers

Quantum-dot (QD) metal-cavity surface-emitting microlasers were designed, fabricated, and characterized recently [4] for various sizes of cavity volume for both lateral and vertical confinements. Microlasers using submonolayer quantum dots in the active region are fabricated according to our design model optimized for a resonant metal cavity. The cavity-volume scaling law is studied by our theoretical modeling and experimental demonstration as shown in Fig. III.7. The smallest laser has a diameter of 1-μm with silver metal cladding operating at room temperature with electrical injection in pulsed mode. Our experimental results show significant self-heating effect in the smaller devices with a diameter of a few micrometers due to high series resistance and high threshold gain. With the use of hybrid metal-DBR mirrors, the number of DBR pairs in the top hybrid mirror can be reduced from 19.5 to 5.5 without sacrificing threshold current density.

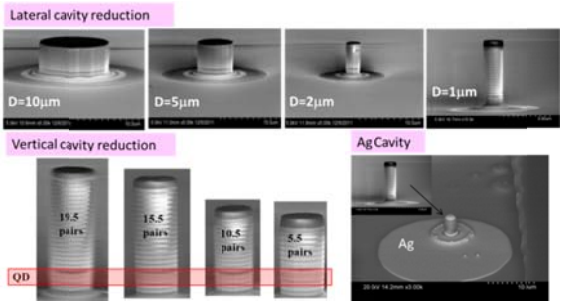

Figure III.7 SEM images of QD metal-cavity surface emitting microlasers. Top pictures show different diameters of micro-pillars post. Bottom: different numbers of the top DBR pairs (left) and conformal silver coverage around the micro-pillar to form three dimensional hybrid metal cavity (right).

References for Section III:

[1] C. Y. Lu, S. L. Chuang, A. Mutig, and D. Bimberg, "Analysis and Demonstration of a metal-cavity surface-emitting microlaser using hybrid metal-DBR reflection," *Opt. Lett.* vol. 36, pp. 2447-2449, 2011.

[2] A. Matsudaira, C. Y. Lu and S. L. Chuang, "Demonstration of metallic nano-cavity emitters with electrical injection," CLEO Baltimore, Maryland, May, 2010

[3] C. Y. Lu and S. L. Chuang, "A surface-emitting 3D metal-nanocavity laser: proposal and theory," Opt. Express **19** (14), 13225-13244 (2011)

[4] A. Matsudaira1, C.Y. Lu, M. Zhang, S. L. Chuang, E. Stock, and D. Bimberg, IEEE Photon. J., 2012

IV. Monolithic Nanolasers on Silicon (Connie Chang-Hasnain)

IV.1 Introduction

Augmenting electronics with photonics is expected to enable new capabilities in myriad fields including computing, communications, sensing, and medical diagnostics. Active photonic devices typically employ III-V materials because of their superior optical properties. Meanwhile, the foundation of electronics is silicon (Si), an optically-deficient semiconductor. Physically merging these two materials therefore provides a natural pathway towards creating optoelectronic functionality. However, prominent dissimilarities in basic material properties like lattice constant have severely inhibited such integration. Furthermore, the nanoscale nature of modern transistors demands complementary nanophotonics that approach or even break subwavelength limits of light. Here, we leverage a unique CMOS-compatible growth process that populates silicon wafers with single-crystal GaAs-based nanopillars. With these nanostructures, we have realized monolithic nanolasers on silicon under optical pumping. Under electrical injection, nanopillars exhibit amplified spontaneous emission, representing a major step towards the first silicon-based diode nanolasers.

IV.2. Material growth and device fabrication

GaAs-based nanopillars were grown without catalysts on (111) silicon using metal-organic chemical vapor deposition (MOCVD) at a low temperature of 400 °C, thereby achieving compatibility with strict CMOS foundry processes. This provides a critical advantage for scalability of nano-optoelectronics. By controlling doping and composition during core-shell growth, we created radial p-i-n heterostructures as schematized in Fig. IV 1(a). Figure IV.1(b) shows a scanning electron microscope (SEM) image of the as-grown nanomaterials. Typically, the core of the nanopillar is nominally n-type $In_{0.12}Ga_{0.88}As$ followed by an intrinsic $In_{0.3}Ga_{0.7}As$ active layer. The cladding consists of thin layers of i-GaAs and p-GaAs, which provide surface passivation and the device p-contact layer, respectively. Additional details on growth can be found in ref. [1–3]

To fabricate nanopillar devices, a series of lithography, etching, and deposition steps were

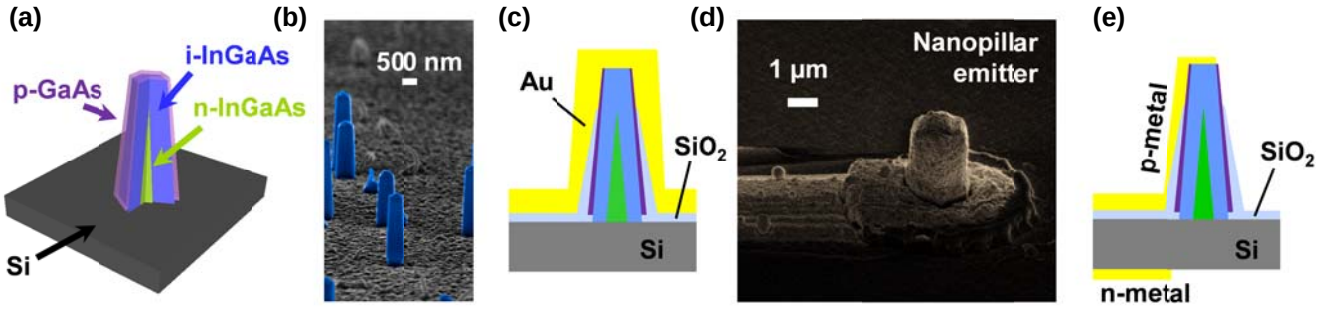

Fig. IV.1. (a) Schematic of a III-V nanopillar on silicon with radial p-i-n heterojunctions. Core-shell growth and control of doping and composition enable these structures. **(b)** SEM images of as-grown nanopillars prior to processing. Various etching, lithography, and deposition techniques were used to fabricate nanopillar devices. Schematics and SEM images are respectively shown in **(c)** and **(d)** for nanopillar laser structures and in **(e)** and **(f)** for APDs. SiO_2 acts as electrical insulation between the p- and n-type layers. Two top-side test pads were used for high-speed APD testing.

used. Both electron beam and standard microfabrication techniques were employed. When fully encapsulated in carefully designed layers of SiO_2 and Au, nanopillars become metal-optic resonators as shown in Figs. IV.1(c) and 1(d). If an optical window is opened as shown in Figs.IV.1(e), nanopillar devices can function as both light-emitting diodes and avalanche photodiodes (APDs), depending on the polarity of electrical bias. Thus, nanopillars offer a great deal of flexibility for applications; simple modifications to the fabrication process can result in numerous nanophotonic device permutations.

IV.3 Lasers and LEDs on silicon

Because nanopillars are extremely well-faceted, they form natural on-chip optical cavities immediately after growth without any additional processing. Under optical pumping, nanopillars on silicon reach full laser oscillation up to room temperature and with subwavelength dimensions [4]. Relatively broadband spontaneous emission is seen from nanopillars below threshold. As the pump fluence increases, band filling effects are seen until a cavity peak emerges and full laser oscillation is achieved as shown in Fig. IV.2(a). Strong coherence of nanopillar emission can be seen from a high suppression ratio of 17 dB in the lasing spectra as well as prominent speckles in near field images.

Achieving sufficient optical feedback is not intuitive given that the back facet, i.e. the nanopillar and Si interface, sees hardly any index contrast. Conventional thinking suggests that there would be insufficient reflectivity as well as severe absorption loss due to the smaller Si band gap. However, we find that optical fields can be tightly confined in nanopillars by helically propagating modes that are cut off and reflected at the interface with silicon [4]. Light output as a function of pump fluence (L-L curve) is shown in a Fig. 2(b), showing a distinct threshold at 22 $\mu J/cm^2$. Fitting the L-L curve reveals β~0.01 and experimental Q~200. Theoretical studies have shown that these modes can have Q factors reaching several thousand even for subwavelength structures [4].

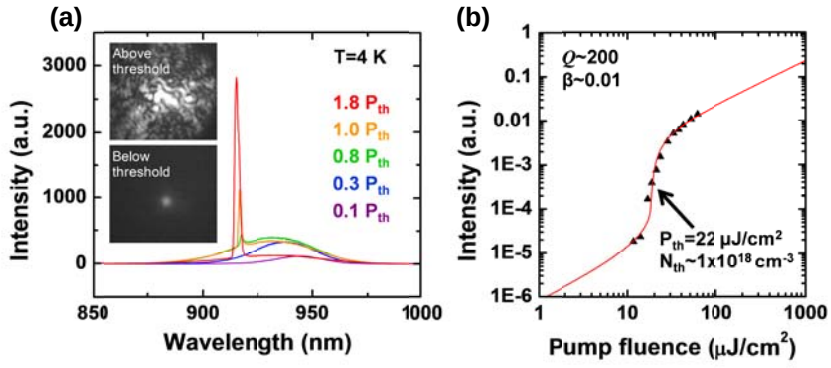

Fig. IV. 2. (a) Nanopillar emission spectra are shown at various pumping levels ($0.1P_{th}$ – $1.8P_{th}$). Evolution of the lasing peak can be clearly seen. In the insets, optical images show the appearance of speckle patterns due to optical coherence when the laser is biased above threshold. **(b)** The pump-dependence of nanopillar light output reveals a clear lasing threshold of 22 $\mu J/cm^2$. From analysis of this curve and associated spectra, we calculated the quality and spontaneous emission coupling factors as Q~200 and β~0.01,

True nano-optoelectronic functionality requires electrical control of nanophotonic devices. When electrically contacting nanopillars, the presence of metal severely perturbs cavity modes of such small structures. Thus, a great deal of care is needed in designing an electrical injection

structure that simultaneously supports optical resonances. Here, metal-optics provides an attractive feedback mechanism for small lasers because it offers small mode volumes [5–7]. In this case, metal contacts can then conveniently double as optical reflectors. By embedding nanopillars in a metal-optic cavity (see Figs. IV.1(c) and 1(d)), we have now achieved amplified spontaneous emission driven by electrical bias. To test the devices, samples were wire bonded onto chip carriers mounted inside a liquid helium cryostat with optical access. Electrical feedthroughs connected devices to a pulse generator in the external environment. 20 ns pump pulses with a 10 μs period were delivered in these experiments. An objective collected electroluminescence (EL), which was then relayed to a spectrometer and CCD for detection.

Cavity peaks can be seen superimposed on a broad spontaneous emission background under high injection levels (up to 700 μA) as shown in Fig. IV. 3(a). In order to ascertain the origin of the EL peaks, temperature dependence studies were carried out. The shift versus temperature of the purported cavity peaks and the overall EL spectrum are plotted in Fig. IV.3(b). Notably, peaks A, B, C, and D all shift at the same rate, while the overall EL spectrum (X) shifts more strongly. This can be explained by the

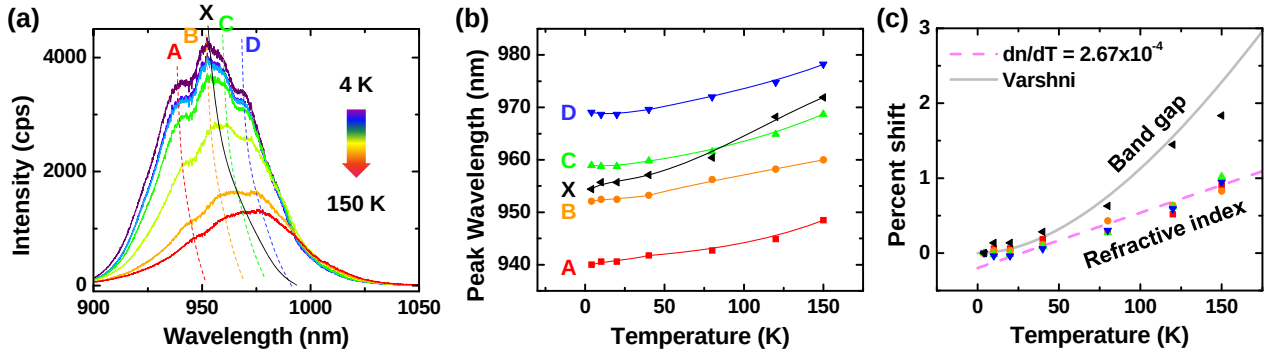

Fig. IV.3. (a) Electrically-injected emission spectra show several ASE peaks (A-D) superimposed upon a broad spontaneous emission background (X). Temperature dependence studies were done to verify the origin of these peaks. **(b)** Spontaneous emission (X) shifts more quickly with temperature than the purported cavity peaks (A-D), which shift in parallel with one another. **(c)** This can be explained by the different temperature dependences of band gap energy and refractive index, which determine energy shifts of spontaneous emission and cavity resonances, respectively. We find that peak X follows the Varshni model for energy band gaps, while peaks A-D follow a typical GaAs thermo-optic coefficient of $dn/dT=2.67\times10^{-4}$. We thereby confirm our attribution of observed spectral peaks to ASE.

stronger temperature dependence of band gap energy compared to refractive index. When plotting the wavelength shifts as percentages as in Fig. IV. 3(c), we can compare our results to well-known and existing models. We find that the ASE peaks shift at a rate corresponding to a typical GaAs thermo-optic coefficient of $dn/dT=2.67\times10^{-4}$, thereby substantiating their origin from cavity modes since optical resonances are linearly dependent on refractive index. Meanwhile, peak X follows the Varshni model known for describing the temperature dependence of semiconductor band gaps. We note that there is a deviation from the Varshni model at higher temperatures, which is a topic of future investigation. From other analyses, we found that we currently achieve a material gain of 3,400 cm^{-1}. This agrees with the exceptional electrical properties we have observed. Device dark current is only 1.2 pA and 0.45 nA at 0 V and -1 V, respectively. Nanopillar devices have textbook IV characteristics with nearly-ideal

ideality factors of 2. A material gain of 3,400 cm^{-1} is sufficient for reaching typical lasing thresholds; thus, our structure is presently limited by insufficient optical feedback or *Q*. Nonetheless, the observation of ASE from nanopillars grown on silicon is a major step towards realizing the ultimate monolithic silicon-based light source.

IV.4 Outlook

As computing power continues to centralize in the form of data centers, chip-level data transport capacity becomes increasingly critical. Using silicon nanophotonics to implement low-power optical interconnects is a promising approach to solving impending bandwidth limitations. To offer advantages over electrical interconnects, optical devices must be extremely efficient, and their integration onto Si has to be highly scalable. Nanolasers such as the ones presented above therefore offer an extremely attractive solution. With subwavelength physical volumes, nanolasers minimize power consumption while still achieving strong monochromatic emission, though sufficient power and beam control remain areas requiring further development. On a higher level, the variety of nanolasers achieved by our team has created a class of photonic devices opening new functionality beyond the scope of traditional lasers. Controllably interfacing photons with nanoscale matter such as atoms, molecules, nanoparticles, and fullerenes is no longer a fantasy, but instead a reality on the horizon.

References for Section IV

[1] M. Moewe, L. C. Chuang, S. Crankshaw, C. Chase, and C. Chang-Hasnain, "Atomically sharp catalyst-free wurtzite GaAs/AlGaAs nanoneedles grown on silicon," *Appl. Phys. Lett.*, vol. 93, no. 2, pp. 023116–3, Jul. 2008.

[2] L. C. Chuang, M. Moewe, K. W. Ng, T.-T. D. Tran, S. Crankshaw, R. Chen, W. S. Ko, and C. Chang-Hasnain, "GaAs nanoneedles grown on sapphire," *Appl. Phys. Lett.*, vol. 98, no. 12, p. 123101, 2011.

[3] M. Moewe, L. C. Chuang, S. Crankshaw, K. W. Ng, and C. Chang-Hasnain, "Core-shell InGaAs/GaAs quantum well nanoneedles grown on silicon with silicon-transparent emission," *Opt. Express*, vol. 17, no. 10, pp. 7831–7836, May 2009.

[4] R. Chen, T.-T. D. Tran, K. W. Ng, W. S. Ko, L. C. Chuang, F. G. Sedgwick, and C. Chang-Hasnain, "Nanolasers grown on silicon," *Nat Photon*, vol. 5, no. 3, pp. 170–175, Mar. 2011.

[5] M. T. Hill, Y.-S. Oei, B. Smalbrugge, Y. Zhu, T. de Vries, P. J. van Veldhoven, F. W. M. van Otten, T. J. Eijkemans, J. P. Turkiewicz, H. de Waardt, E. J. Geluk, S.-H. Kwon, Y.-H. Lee, R. Notzel, and M. K. Smit, "Lasing in metallic-coated nanocavities," *Nat Photon*, vol. 1, no. 10, pp. 589–594, Oct. 2007.

[6] K. Yu, A. Lakhani, and M. C. Wu, "Subwavelength metal-optic semiconductor nanopatch lasers," *Opt. Express*, vol. 18, no. 9, pp. 8790–8799, Apr. 2010.

[7] M. P. Nezhad, A. Simic, O. Bondarenko, B. Slutsky, A. Mizrahi, L. Feng, V. Lomakin, and Y. Fainman, "Room-temperature subwavelength metallo-dielectric lasers," *Nature Photonics*, vol. 4, no. 6, pp. 395–399, Apr. 2010.

[8] A. V. Krishnamoorthy, K. W. Goossen, W. Jan, X. Zheng, R. Ho, G. Li, R. Rozier, F. Liu, D. Patil, J. Lexau, and others, "Progress in low-power switched optical interconnects," *Selected Topics in Quantum Electronics, IEEE Journal of*, no. 99, pp. 1–20, 2011.

[9] D. A. B. Miller, "Device Requirements for Optical Interconnects to Silicon Chips," *Proc. IEEE*, 2009.

Addendum-2013-Part I

NACHOS Report: Plasmonic Nanolasers (CunZheng Ning)

1. Executive Summary

Metallic and plasmonic based nanostructures promise to allow miniaturization of photonic devices down to unprecedented levels. The efforts reported here covers the electrical injection plasmonic-semiconductor nanolasers and plasmonic emitters. Major achievements involve the first realization of a nanolaser with size smaller than wavelength in vacuum in *all three* dimensions, operating at room temperature under electrical injection. The team remains the only group in the world capable of doing this almost a year after they achieved these critical milestones. Several other interesting devices were also demonstrated for the first time during the period of performances including the first electrical injection, direct generation of an azimuthally polarized laser light, and the first demonstration of electrical injection light emission from an integrated semiconductor-metallic bowtie structure. These demonstrations illustrate the great potential of plasmonic-semiconductor nanostructures in their versatility for many other applications.

The novelty of our research and significance of progress made were also evidenced by great attention our research received from technology and popular press, including interviews, news reports, and press highlights in many journals, magazine, and websites. Following pages contain more detailed description of progress made and the major results.

2. Background

Nanophotonics deals with generation, control, and manipulation of photons at nanometer scale with eventual goals of achieving photonic integrated systems on a chip and the final grand integration with electronics on a chip. To achieve such a system on a chip, it is critical to achieve various light sources and other active devices at nanometer scale on a chip. Surface-plasmon polariton (SPP) formation is one of the most important mechanisms to confine light at nanometer scale for detection, sensing, and communication, and thus has become one of the most critical elements for on-chip photonic integrated system. During the performance period, research was carried out to develop an electrical injection SPP hotwire sources and plasmonic nanolasers.

Surface Plasmon Polariton and its generation

With the rapid progress in nanoscale fabrication capability and in our understanding of the interaction between light field and nano-metallic structure, it has become possible to design and fabricate truly nanophotonic devices to confine optical field in an extremely small space dimensions, on the order of a small fraction of the wave-length of the corresponding dielectric medium. One of the very prominent examples of such capability is the first demonstration of a semiconductor nanolaser with a thickness below the diffraction limit, carried out by the PI's group and his collaborators. However, the demonstrated nanoscale lasers could only operate at very low temperature. It is extremely important for many practical applications to be able to operate such nanolasers at room temperature. In addition, among the metallic structures proposed to confine light field or generate plasmonic near field sources, metallic bowtie pairs are shown to

be able to confine light in the smallest space and with the highest field enhancement between the bowtie tips. Though bowtie structures have been studied quite extensively, lack of a device concept and a method of fabrication to integrate bowtie structure with active materials in a reproducible manner and in a controllable way prevent these advantages from being incorporated into device applications. Moreover, the current prevailing method of generating such SPP modes is using optical pumping. The requirement of phase matching and a large external pump laser required makes optical generation intrinsically incompatible with the intended future on-chip applications. Thus the focus of our research in the area of plasmonic nanoemitters is to achieve room temperature operation of a nanolaser under electrical injection and on electrical injection operation of bowtie emitters as a potential plasmonic source.

3. Description of Major Research Results

3.1 First Room Temperature Electrical Injection Nanolaser finally Demonstrated:

Achieving electrical injection nanolasers with a size smaller than wavelength in 3D capable of operating at room temperature has been a goal actively pursued worldwide over the laser few years. Due to the small size of such nanolasers, the fabrication precision required is extremely challenging to achieve high quality devices, capable of room temperature operating. We are the first group to finally achieve this long sought goal recently, as shown in Fig.1. So far nearly 9 months after the publication of our results, we are still the only group being able to do this. The results have been widely reported world-wide by tech press and news media in general. This achievement represents a major milestone in the development of metallic cavity nanolasers and in terms of possible real world application of such nanolasers. Currently similar research is actively pursued worldwide.

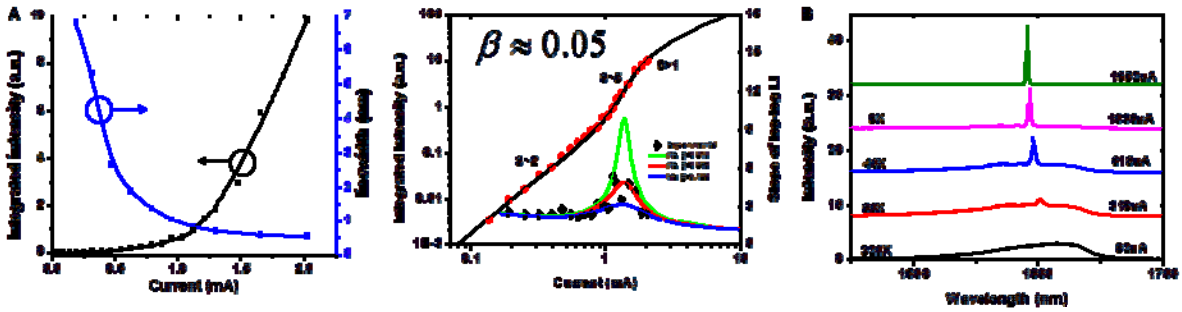

Figure 1 Room temperature perating characteristics of a semiconductor metallic cavity nanolaser of subwavelength in size. Left: L-I curve (left axis) and linewidth vs. current (right axis) showing the standard threshold behavior of linewidth reduction with pumping current with the narrowest linewidth around 0.5 nm. This is the smallest linewidth demonstrated for a metallic cavity nanolaser. The L-I curve is plotted on log-log scale in the middle panel, showing the typical S-curve. The right panel shows the spectra at increasing pumping levels. All three panels show convincingly that the lasing has occurred in such a laser. The size of this laser: 1.15 (W) × 1.39 (L) × 1.5 (H) μm^3 = 0.67 λ^3 (λ=1591 nm).

During the period of the performance, we have been leading the community over the last few years with either the smallest electrical injection lasers, or operating at the highest temperature. Various other interesting results were obtained also including the first purely electrical injection azimuthally polarized laser source. Our results have been published in several research papers and in various invited review articles as listed in the following:

- Ding K, Hill MT, Liu ZC, Yin LJ, Veldhoven PJV, Ning C.Z., **Record performance of electrical injection sub-wavelength metallic-cavity semiconductor lasers at room temperature**, Opt. Express, 21, 4728-4733(2013)
- K. Ding and C. Z. Ning, **Metallic subwavelength-cavity semiconductor nanolaser**. (an invited review). Light: Science and Applications, 1(7),e20(2012); doi:10.1038/lsa.2012.20
- D. Li and C.Z. Ning, **Interplay of various loss mechanisms and ultimate size limit of a surface plasmon polariton semiconductor nanolaser**, Opt. Exp., 20, 16348-16357 (2012)
- K. Ding, Z.C. Liu, L.J. Yin, M. T. Hill, M. J. H. Marell, P. J. van Veldhoven, R. Nöetzel, C.Z. Ning, **Room Temperature Continuous Wave Lasing in Deep-Subwavelength Metallic-Cavities under Electrical Injection**, Phys. Rev. B85 (Rapid Communication), 041301(2012)
- K. Ding, Zhicheng Liu, Leijun Yin, Hua Wang, Ruibin Liu, Martin T. Hill, Milan J. H. Marell, Peter J. van Veldhoven, Richard Nötzel, and C. Z. Ning, **Electrical injection, continuous wave operation of subwavelength-metallic cavity lasers at 260 K**, Kang, ***Appl. Phys. Lett.***, **98**, 231108, 2011.
- K. Ding and C.Z. Ning, Fabrication challenges of electrical injection metallic cavity semiconductor nanolasers (invited paper), Semicond. Sci. Technol., accepted, (2013)
- K. Ding, M. Hill, Z.C. Liu, L. J. Yin, P. J. van Veldhoven, and C.Z. Ning, An electrical injection metallic cavity nanolaser with azimuthal polarization Lasers, Appl. Phys. Lett., 102, 041110 (2013); doi: 10.1063/1.4775803

3.2 Electrical injection metallic-semiconductor bowtie plasmonic emitters demonstrated:
Bowtie structure has been a prototype of a plasmonic emitter due to the strong enhanced field

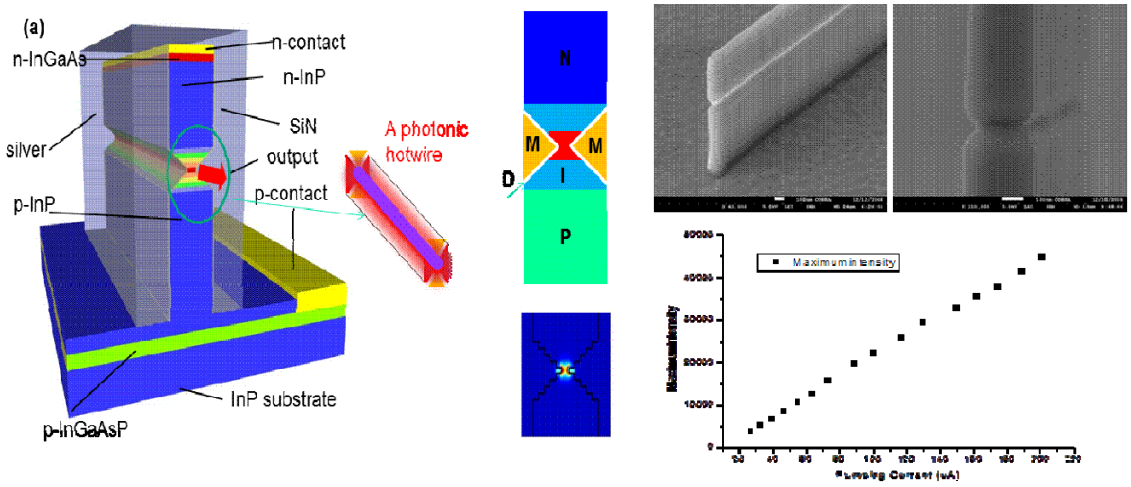

Figure 2: Left: schematic of the electrical injection metallic bowtie plasmonic emitter; Middle: schematic of the cross section (top) and simulated field distribution (bottom); Right panel: SEM image of semiconductor bowtie pillar (top) and L-I curve of experiment measurements of the light output from the side after cutting by a focused ion beam from the side.

near the bowtie tips. But the effectiveness of such structure requires the active gain medium be positioned in between the bowtie tips. Such an arrangement represents a fabrication challenge. So far people have not been able to do this reliably by other bottom-up approaches. While carrying out our plasmonic nanolaser research, we realized that a one-step fabrication based on top-down lithography could allow the fabrication of the metallic bowtie structure and the integration with gain medium, potentially allowing such structures be fabricated using standard device fabrication tools and processes. Fig. 2 (right) shows a scanning electron microscope (SEM) image of a semiconductor pillar etched from an InP/InGaAsP wafer. The bowtie-shaped groves etched into semiconductor pillar will serve as a template for later deposition of metals (such as Au and Ag), so that metallic bowtie pairs will be formed in the middle of the pillar, where wafer growth defines semiconductor gain region between and around bowtie tips, creating a closely and precisely positioned and strongly coupled metal-semiconductor bowtie system, ideal for generating intense SPP near field. Since the InP wafer has built-in doped and contact layers, electrical injection can be readily accomplished, leading to a natural on-chip SPP generation without the need of bulk optical pumping. We have recently used the similar fabrication process to demonstrate the first ever sub-diffraction limit laser. The light emission has been measured from such structure as shown in Fig. 2 (low right). For more info, see, K. Ding, H. Wang, M. T. Hill, and C. Z. Ning, Design and fabrication of an electrical injection metallic bowtie plasmonic structure integrated with semiconductor gain medium, App. Phys. Lett., 102, 041110 (2013); doi: 10.1063/1.4775803

3.3 First demonstration of a nanolaser with azimuthal polarization: Light beams with various special polarizations have important applications such as polarized along radial or azimuthal directions. Typically such beams have to be generated by special gratings or by external polarization selection after devices been fabricated. For many applications, a single integrated device would be preferred. Our nanolasers with cylindrical symmetries (see Fig.3) are ideal for such polarized beam generation. We demonstrated for the first time an azimuthally polarized laser source from an electrically driven metallic cavity nanolaser with a physical cavity volume of 0.146 λ^3 (λ = 1416 nm). Single TE01 mode lasing at 78 K was achieved by taking the advantages of the large free spectral range in such nanoscale lasers and the azimuthal polarization of lasing emission was verified experimentally (see Fig.4). Mode shift controlled by device cavity radius was observed over a large wavelength range from 1.37 μm to 1.53 μm. Such metallic cavity nanolaser provides a compact electrically driven laser source for azimuthally polarized beam. Fig.3 shows the schematic laser structure and the SEM image of the fabricated pillar. Fig. 4 shows the L-I curve (a) and spectrum (inset of (a)), the lasing mode shift with pillar diameter, and polarization

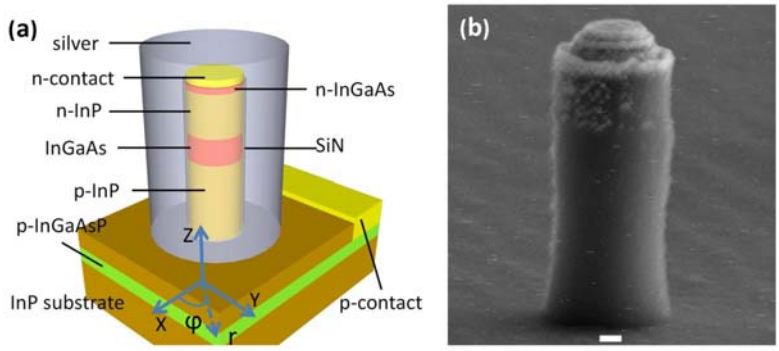

Figure 3: (a) Structure of a metallic cavity nanolaser with circular cross section. (b) Scanning electron microscope image of an InP/InGaAs/InP nano-pillar coated with SiN layer on its sidewall. We etched away the SiN on top of the pillar and deposited Ti/Pt/Au thus forming the top n contact. Scale bar is 100 nm.

resolved imaging. The dark line in the images along the direction of the polarizer is the evidence of the azimuthal polarization.

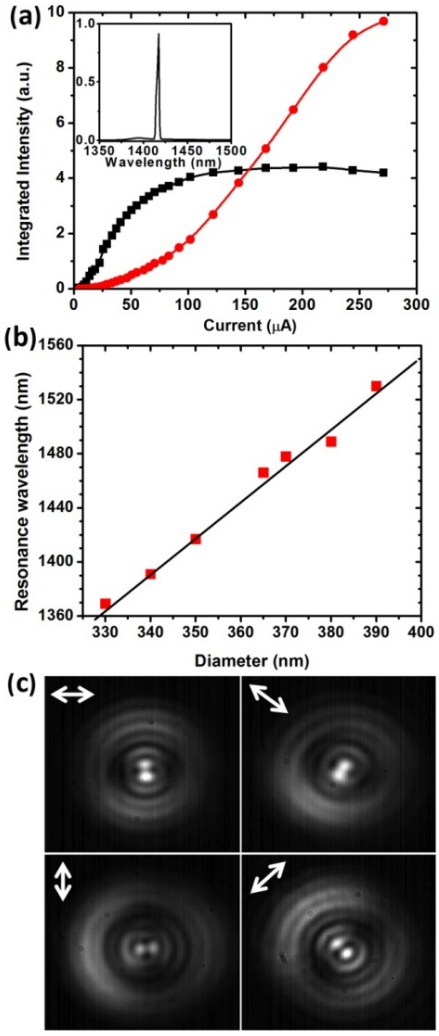

4. Awards and Prizes

C.Z. Ning, Elected to Fellow of The Optical Society, 2012, due to significant contribution to nanophotonics

C.Z. Ning, Elected to be Fellow of IEEE, 2012, due to his significant contribution to nanophotonics

C.Z. Ning, OSA Fellow Lecturer Award, 2013

5. Invited Talks on the Research Results

1) C.Z. Ning, Kang Ding, **Recent Progress in Metallic Cavity Nanolasers**, Invited Talk at IEEE Photonics Society Summer Topical Meetings, Hawaii, July 2013
2) C.Z. Ning, **Recent Progress in Metallic Cavity Nanolasers**, invited talk at IEEE Photonics Society Annual Meeting (IPC), Seattle, WA, Sept 7-12, 2013
3) C.Z. Ning, **Metallic Cavity Nanolasers: A New Paradigm for Semiconductor Lasers**, invited Lecture at International Nano-Optoelectronics Workshop (iNOW), Aug 20-Aug 30, 2013, Corsica, France
4) C.Z. Ning, K. Ding, D. B. Li, L.J. Yin, and Z.C. Liu, **Surface Plasmonics and Metallic Cavity Nanolasers**, invited talk at PIERS 2013, Stockholm, Aug 12-15
5) C.Z. Ning, **Plasmonic Nanolasers: A Paradigm Shift in Laser Physics,** Physics Colloquium and SFB 787 Seminar, May 16, 2013
6) C.Z. Ning, **Plasmonic Nanolasers: Towards the Ultimate Miniaturization,** Invited Talk, Semiconductor and Integrated OptoElectronics (SIOE) Conference April 9-11th 2013, Cardiff,UK
7) C.Z.Ning, **Loss Compensating and Lasing in Sub-wavelength Semiconductor-Metal Structure**s, Department of Physics, Imperial College London, UK, April 12, 2013
8) C.Z. Ning, **Plasmonic and Metallic Cavity Semiconductor Nanolasers,** HP Lab, April 4, 2013
9) C.Z. Ning, **Semiconductor Nanowires for Photonic Applications from Ultraviolet to Mid-infrared,** ASU Nano Science Seminar Series, April 1, 2013
10) C.Z. Ning, **Nanolasers: Current Status of Trailblazer of Synergetics**, *International Symposium*: *Self-Organization in Complex Systems: The Past, Present, and Future*

of Synergetics, (on the ocassion of Hermann Haken's 85th birthday), Delmenhorst, Germany, Nov 13-16, 2012

11) C.Z. Ning, **Nanophotonics with Nanowires and Plasmonics**, Keynote talk, at The SecondInternational Conference on Manipulation, Manufacturing and Measurement on the Nanoscale, 29 August –1 September2012, Xi'an, China

12) C.Z. Ning, **Nanophotonics with Nanowires and Plasmonic Shells**, Hong Kang Polytech University, May 22, 2012

13) C.Z. Ning, **Photon-Plasmon Interactions and Subwavelength Nanolasers**, Physics Colloquium, Shanghao Jiaotong University, May 30, 2012

14) C.Z. Ning, **Two-Photon Lasers in Semiconductors**, talk at Physics Department, Shanghai Jiaotong University, May 30, 2012

15) C.Z. Ning, **Semiconductor Alloy Nanowires for Optoelectronic Applications from UV to IR**, Seminar at School of Nanoscience and Technology, Suzhou University, Suzhou, China, June 4, 2012

16) C.Z. Ning, **Semiconductor Alloy Nanowires and Plasmonic Nanostructures for Nanophotonics**, Colloquium of Department of Optoelectronics, Zhejiang University, Hangzhou, China, June 7, 2012

17) C.Z. Ning, **Photon-Plasmon Interactions and Subwavelength Nanolasers**, Condensed Matter Seminar Series, Physics Department, Peking University, June 20, 2012

18) C.Z.Ning, **Composition Graded II-VI and IV-VI Nanowires for Full-Spectrum Optoelectronic Applications from UV to Mid-IR**， InternationalWorshop on 6.1A II-VI and III-V Materials and Their Integration, Tempe, AZ, Nov 2011

19) C.Z. Ning, **Semiconductor Alloy Nanowires for Optoelectronics Applications from UV to Midinfrared,** Material Science Seminar, University of Wisconsin Madison, Sept 29, 2011

20) C.Z. Ning, **Plasmonic nanolasers with subwavelength-size cavities: progress and prospects**, International Nano-Optoelectronics Workshop (iNOW 2011), St-Petersburg-Wurzburg, July 26-Aug 5, 2011

21) C.Z. Ning, **Plasmonics with Semiconductors: Loss Compensation and Lasing**, ICMAT 2011, Singapore, June 29, 2011

22) C.Z. Ning**, Plasmonic Nanolasers with Sub-Wavelength-Size Cavities: Progress and Perspectives**, International Conference on Nanophotonics, Shanghai, China, May 22-26, 2011

23) Cun-Zheng Ning, Derek Caselli, Ding Kang, Debin Li, Zhicheng Liu, Patricia L. Nichols, Minghua Sun, Leijun Yin, **Nanophotonics with Plasmonics and Nanowires: Applications to Subwavelength Lasers and Novel Solar Cells**, Villa Conference on Interactions Among Nanostructures, April 21-25, 2011 Las Vegas, Nevada

24) Z. Liu, K. Ding, L. Yin, M. Hill, M.J. Marell, R.J. van Veldhoven, R. Noetzel, C. Z. Ning, **Room Temperature CW Operation of Metal–Semiconductor Plasmonic Nanolasers with Subwavelength Cavity**,CLEO/QELS, Baltimore, MD, May 2-6, 2011

25) C.Z. Ning, **Alloy semiconductor nanowires for optoelectronic applications from UV to IR**, March 16, 2011, Lecture, EECS Department, UC Berkeley

26) C.Z. Ning, **Semiconductor alloy nanowires and applications to high efficiency solar cells**, AZ Nanotech Council, Feb 24, 2011

27) C.Z. Ning, **Nanophotonics with Plasmonics and Nanowires: Applications to Subwavelength Lasers and Novel Solar Cells,** Symposium on Nanophotonics and Renewable Energy, Chinese Acandemy of Science, Institute of Physics, Jan 17-18, 2011
28) C.Z. Ning, **Approaching Size Limit of Nanolasers with Wires and Plasmonic Shells**, ECE Colloquium, University of Illinois at Urbana Champaign, Oct 14, 2010

6. Papers published under the DARPA support:

[1] Ding K, Hill MT, Liu ZC, Yin LJ, Veldhoven PJV, Ning C.Z., **Record performance of electrical injection sub-wavelength metallic-cavity semiconductor lasers at room temperature**, Opt. Express, 21, 4728-4733(2013)

[2] K. Ding, H. Wang, M. T. Hill, and C. Z. Ning, **Design and fabrication of an electrical injection metallic bowtie plasmonic structure integrated with semiconductor gain medium**, App. Phys. Lett., 102, 041110 (2013); doi: 10.1063/1.4775803

[3] K. Ding and C.Z. Ning, **Fabrication challenges of electrical injection metallic cavity semiconductor nanolasers (invited paper),** Semicond. Sci. Technol., accepted, (2013)

[4] C.Z. Ning, **What is Laser Threshold**?, (invited paper), J. Special Topics of Quantum Electronics, **19**, 1503604 (2013)

[5] K. Ding, M. Hill, Z.C. Liu, L. J. Yin, P. J. van Veldhoven, and C.Z. Ning, **An electrical injection metallic cavity nanolaser with azimuthal polarization Lasers**, Appl. Phys. Lett., 102, 041110 (2013); doi: 10.1063/1.4775803

[6] C.Z. Ning, **Nanolasers: Current Status of The Trailblazer of Synergetics**, in *Self-Organization in Complex Systems: The Past, Present, and Future of Synergetics,* eds. A. Pelster and G. Wunner, (Springer, 2013)

[7] X. Wu, Y. Xiao, C. Meng, X. Zhang, S. Yu, Y. Wang, C. Yang, X. Gu, C. Z. Ning, L.M. Tong, **Longitudinal hybrid photon-plasmon nanowire lasers**, Nano Lett., Article ASAP, DOI: 10.1021/nl403325j, October 17, 2013

[8] K. Ding and C. Z. Ning, **Metallic subwavelength-cavity semiconductor nanolaser**. (an invited review). Light: Science and Applications, 1(7),e20(2012); doi:10.1038/lsa.2012.20

[9] D. Li and C.Z. Ning, **Interplay of various loss mechanisms and ultimate size limit of a surface plasmon polariton semiconductor nanolaser**, Opt. Exp., 20, 16348-16357 (2012)

[10] K. Ding, Z.C. Liu, L.J. Yin, M. T. Hill, M. J. H. Marell, P. J. van Veldhoven, R. Nöetzel, C.Z. Ning, **Room Temperature Continuous Wave Lasing in Deep-Subwavelength Metallic-Cavities under Electrical Injection**, Phys. Rev. B85 (Rapid Communication), 041301(2012)

[11] K. Ding, Zhicheng Liu, Leijun Yin, Hua Wang, Ruibin Liu, Martin T. Hill, Milan J. H. Marell, Peter J. van Veldhoven, Richard Nötzel, and C. Z. Ning, **Electrical injection, continuous wave operation of subwavelength-metallic cavity lasers at 260 K**, Kang, ***Appl. Phys. Lett.***, **98**, 231108, 2011.

Addendum-2013-Part II

Spectral Manipulation in Nanowire Lasers (Peidong Yang)

Nanowires have been identified as potential building blocks that mimic conventional photonic components such as interconnects, waveguides, and optical cavities at the nanoscale[1-3]. Semiconductor nanowires with high optical gain offer promising solutions for lasers with small footprints and low power consumption[4-5]. Although much effort has been directed toward controlling their size[6], shape[7], and composition[8-9], most nanowire lasers currently suffer from being low-quality cavities, a problem that is universal in nanocavities because miniature features induce significant optical loss. Because of this difficulty, it remains an outstanding challenge to rationally control the spectra of room-temperature nano-lasers. Our work focuses on the development of experimental and theoretical strategies to manipulate the lasing modes of a semiconductor nanowire while also improving the performance of the laser.

Previously, lasing operation at a controlled single UV wavelength at room temperature was achieved using a simple coupling scheme, the cleaved-coupled nanowire[10]. The measured lasing spectra and laser threshold are in good agreement with the calculated spectral modes and threshold gain. This agreement between theory and experiment provides design principles for new methods to control nanowire cavities. The cleaved-coupled nanowire concept can be extended further by controllably etching an array of cuts at a specific period. This periodic structure can form a Distributed Bragg Reflector (DBR). A traditional laser cavity often uses mirrored surfaces at the ends of the cavity. DBRs provide an alternative approach to designing controlled reflection by layering areas of alternating high and low index of refraction. They can be fabricated by layering different materials, or grooves can be etched into a material at regular periods. By using focused-ion beam milling, controlled indentations can be etched into the nanowire to create stop bands with high reflectivity of the fundamental waveguide mode (**Fig. 1**).

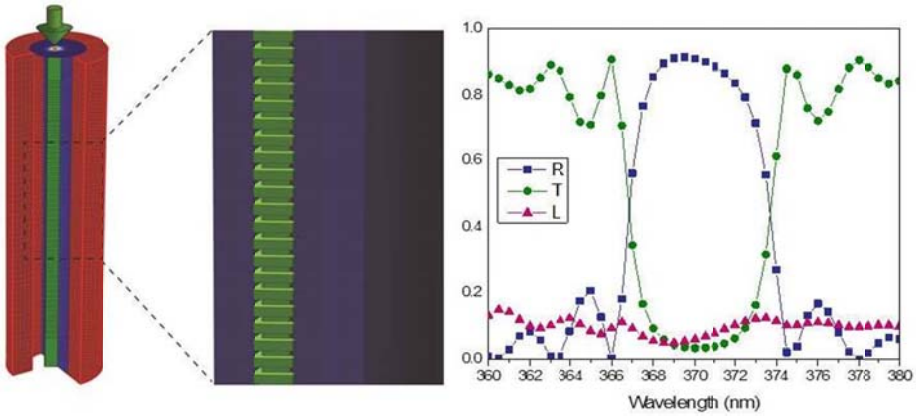

Figure 1. Simulated transmission (T) and reflection (R) of DBR in nanowires. A DBR nanowire (green) lies on top of a silica (dark blue) substrate, backed by perfectly matched layers (red). A narrow photonic band near the wavelength of the GaN bandgap (370 nm) can be observed in both transmission and reflection.

Finite element methods (COMSOL 4.3 Multiphysics) were employed to simulate the optical properties of various DBR structures within a nanowire. In this simulation, the nanowire is 200 nm in radius with triangular cross sections and placed on a SiO_2 substrate, mimicking the actual experimental configuration. The fundamental mode (TM00) was injected from one end, partially reflected through the DBR, and partially transmitted to the other end of the nanowire. The loss (L) can be visualized as the field scattered into free space. The complex reflection and transmission coefficients were extracted by monitoring the electromagnetic wave propagating in the nanowire. The nanowire was surrounded by a cylindrical region (half glass and half air) and enclosed by a perfectly matched layer that absorbs all scattered electromagnetic waves propagating outward. Because each indentation does not cut through the nanowire, a large reflection coefficient (>80%) is observed since the scattering loss is suppressed. It should be noted that the reflection coefficient for the fundamental mode in a conventional single nanowire is ~20%. These results imply that the lasing threshold for a DBR nanowire can be an order of magnitude lower than the lasing threshold for a single nanowire without the DBR. These simulations also suggest that the photonic band gap can be tuned simply by changing the periodicity of the indentation. With these results in mind, DBR structures were fabricated in nanowires using focused-ion beam milling to control the periodicity and the etching depth.

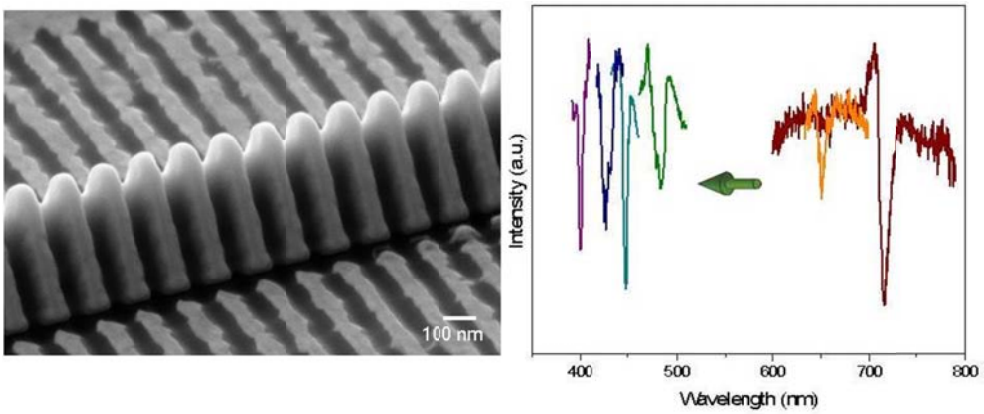

Figure 2. Fabricated nanowire DBR structure and its corresponding spectral response. (**a**) SEM image of a gallium nitride nanowire with etched grooves at a 90-nm periodicity. (**b**) DBR stop bands across the visible spectrum.

To help protect the gallium nitride material, a ~50-nm tungsten metal protection layer is used to coat the nanowire before focused-ion beam milling, and hydrogen peroxide is used to remove the tungsten following the fabrication. The SEM image in Fig. 2 shows a DBR structure with 90-nm periodicity fabricated into a single gallium nitride nanowire. To measure the optical properties of

the DBR structures, a method to perform selected area spectroscopy was developed. One end of the nanowire is excited by a HeCd laser at 325 nm. The emission that passes through the DBR to the other end of the nanowire is collected by a microscope objective (Olympus 60x, N.A. 0.7, in an Olympus inverted optical microscope) and imaged onto a UV-visible spectroscopy spectrometer (Princeton Instruments/Acton) equipped with a 300-groove/mm grating blazed at 500 nm and a liquid N2-cooled charge-coupled device. The recorded spectra are from the light that passes through the DBR. As shown in Fig. 2, photonic stop bands across the entire visible spectrum were observed by adjusting the periodicity of the DBR from 250 nm to 80 nm, the periodicity used to match the band gap emission wavelength. The measured FWHM of the DBR can be less than 10 nm, which illustrates the uniformity and the control of this fabrication procedure. By examining the periodicity with the position of the stop band, the effective index of refraction across the entire visible spectrum for the nanowire can be extracted from the measurement. This method can be potentially applied to other material systems. This compact, one-dimensional architecture is highly reproducible and is anticipated to improve the lasing performance of conventional nanowire lasers.

References:

1. M. Law*, D. Sirbuly*, J. Johnson, J. Goldberger, R. Saykally and P. Yang, *Science*, **305**, 1269 (2004).
2. Y. Li, Q. Fang, J. Xiang and C. M. Lieber. Nanowire electronic and optoelectronic devices. *Mater. Today*, **9**, 18 (2006).
3. R. Yan, D. Gargas and P. Yang, *Nature Phot.*, **3**, 569 (2009).
4. M. Huang, S. Mao, H. Feick, H. Yan, Y. Wu, H. Kind, E. Weber, R. Russo and P. Yang, *Science*, **292**, 1897 (2001).
5. M. A. Zimmler, J. Bao, F. Capasso, S. Muller and C. Ronning, *App. Phys. Lett.*, **93**, 51101 (2008).
6. R. F. Oulton*, V. J. Sorger*, T. Zentgraf*, R.-M. Ma, C. Gladden, L. Dai, G. Bartal and X. Zhang, *Nature*, **461**, 629 (2009).
7. P. Pauzauskie, D. Sirbuly and P. Yang, *Phys. Rev. Lett.*, **96**, 143903 (2006).
8. A. Pan, W.Zhou, E. S. P. Leong, R. Liu, A. H. Chin, B. Zou and C. Z. Ning, *Nano Lett.*, **9**, 784 (2009).
9. F. Qian, Y. Li, S. Gradecak, H.-G. Park, Y. Dong, Y. Ding, Z.L. Wang and C.M. Lieber, *Nature Mater.*, **7**, 701 (2008).
10. H. Gao*, A. Fu*, S. C. Andrews and P. Yang, *Proc. Natl. Acad. Sci. USA*, **110**, 865 (2013).

Addendum-2013-Part III

Nanopatch Laser (Ming C. Wu)

1. Introduction

To reduce the physical size as well as the mode volume of the nanolaser, we have developed a semiconductor nanopatch laser, in which the semiconductor gain media is sandwiched between a metallic nanopatch and a metal ground plane [1][2]. We have developed a versatile platform of realizing many different types of metallodielectric lasers. The fabrication methods developed can be extended for potential integration with CMOS. Both circular and rectangular nanopatch lasers were demonstrated (Fig. V.1).

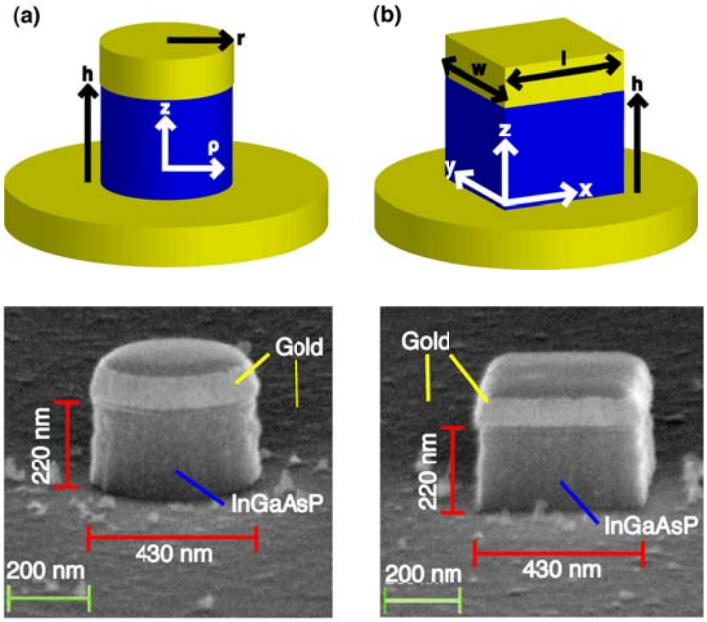

Figure V.1. A schematic and SEM of (a) circular and (b) rectangular nanopatch cavities. Yellow regions represent gold and blue areas signify InGaAsP semiconductor gain media.

Because these lasers operate in near-infrared frequencies, metal behaves more ideally than at visible wavelengths so that plasmonic effects can be neglected and metals can be used in traditional roles (with lower conductivity). Using these metal-optic effects, lasing is achieved in the two modes of a cylindrical resonator, and lasing is achieved in rectangular nanopatch cavities. Physical laser volumes as low as $V_{phys}=0.75\ (\lambda_0/n)^3$ are achieved. We have also made plasmonic crystal laser where the plasmonic action played a key role in the lasing action [3].

2 Experimental Performance of Fabricated Nanopatch Laser

The nanolasers were fabricated using a process that can be compatible with integration onto silicon substrates for applications in optical interconnect technology. In summary, oxide and metal are evaporated onto the epitaxial layer, the substrate is then flipped upside down and bonded to another carrier, mechanical grinding and wet etching techniques are used to remove the backside, the sample is patterned using electron-beam lithography and liftoff, and finally

etched using reactive ion etching. Scanning electron micrographs (SEM) of nanopatch cavities can also be seen in Fig. V.1. More details of the fabrication process can be found in [1].

Lasing from multiple modes of nanopatch cavities is observed. For 220nm thick cavity, lasing is observed from TM_{111} and TE_{011} modes for cylindrical geometries and TM_{011} and TM_{101} modes for rectangular geometries. In cylindrical geometries, the TM_{111} mode is of great interest, since it represents a laser mode with sub-diffraction limited mode and physical volumes (V_n=0.067, V_{phys}=0.75). This so called "electric dipole" mode is also the most fundamental moderate quality factor mode in a cylindrical nanopatch laser. The quality factor is measured to be Q_{exp}=132. The TM_{111} mode has surface normal light emission, much like a VCSEL, and is linearly polarized due to its odd parity. The TE_{011} mode, also called the "magnetic dipole" mode since the electric field lines only have an azimuthal component, also lases. The magnetic mode has larger mode volumes and physical sizes (V_n=0.375, V_{phys}=1.25). The quality factor is measured to be Q_{exp}=168. Temperature dependent quality factors suggest that metal loss is reduced at low temperatures. Data taken from cylindrical nanopatch lasers is summarized in Fig. V.2.

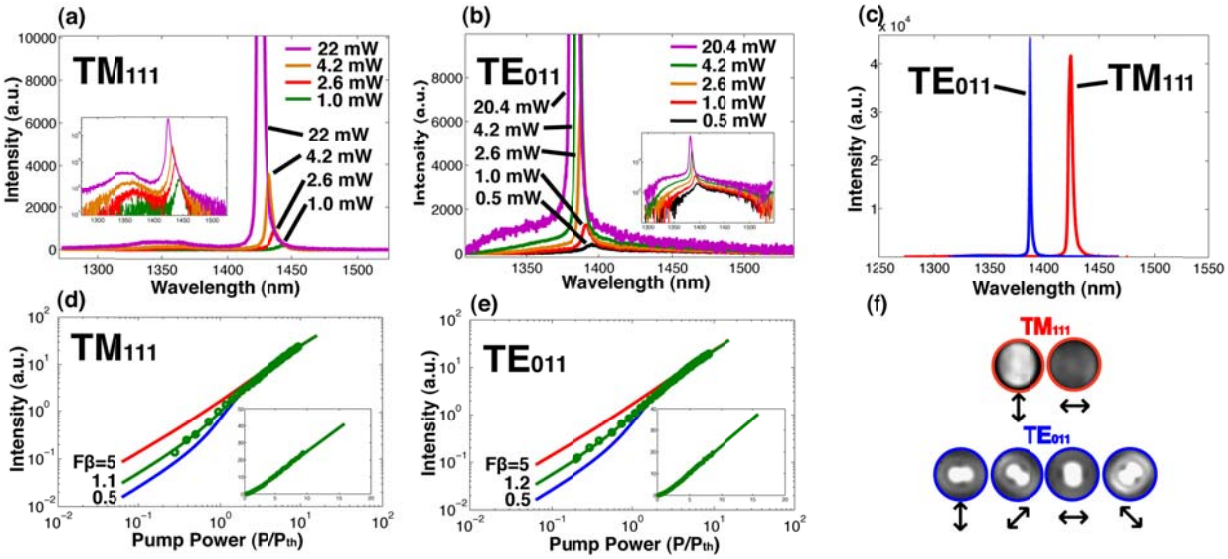

Figure V.2. Pump dependent spectra are shown in linear- and log-scale (inset) for the (a) TM_{111} and (b) TE_{011} cylindrical cavity modes. The linewidths measured are resolution limited above threshold. Linear scale spectra from the two modes just after threshold are seen in (c). Pump-dependent power output of nanopatch lasers are seen in (d) and (e) where rate equation modeled L-L curves are overlaid. Polarization-dependent near field images of each mode confirm each modes identity, with the TM_{111} mode being linearly polarized, and the TE_{011} mode being azimuthally polarized.

Rectangular nanopatches also show lasing action. Two non-degenerate modes with 'electric-dipole-like' mode profiles are seen if the rectangular is anisotropic so that the length is different from the width of the cavity. These devices also have vertical radiation emission. These modes eventually become degenerate as the anisotropy between the length and the width is reduced (Fig. V.3). Between the two modes, the higher energy mode always lases since higher gain can be achieved at higher energies due to a larger density of states. A plot of the mode spacing versus

anisotropy ratio is seen in Fig. V.3(f). There is an overall red shift in cavity resonances only because the cavities probed had larger dimensions at lower anisotropy.

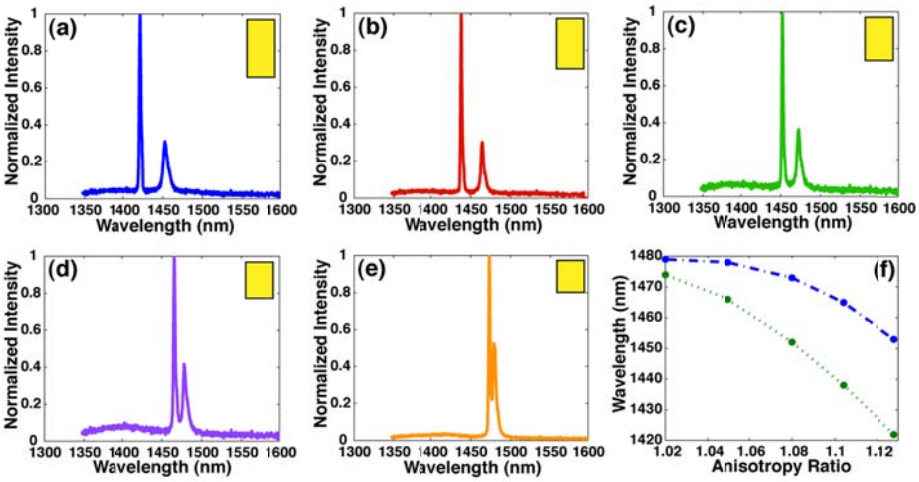

Figure V.3. Nearly lasing spectra for rectangular patches with different anisotropy ratios are shown. The anisotropy ratio is reduced in order from (a) to (e). The yellow rectangles in the corner if each graph signify the top view of each rectangular nanopatch cavity, where the anisotropy has been exaggerated for clarity. The mode separation and wavelength versus anisotropy ratio is seen in (f).

V.3. Coupling to Waveguide and Nanofocusing

The nanolasers can be effectively coupled to integrated waveguide, such as those in Si photonics waveguide with 220nm thickness and about 500nm width. We have shown that with a metallic cavity, the coupling efficiency can be as high as 78% [4], [5]. In addition, the light output can be directly focused onto a nanoscale spot with $2x5nm^2$ area using a metal-insulator-metal plasmonic three-dimensional taper [6], which is directly compatible with the nanopatch laser technology.

V.4. Conclusion

Nanopatch lasers of varying geometries are analyzed, simulated, fabricated, and characterized. These lasers operated in at near-infrared wavelengths, and are smaller than the diffraction limit in both modal and physical volumes. Using metallodielectric cavities at optical frequencies, radiation can be suppressed compared to purely dielectric cavities. Although loss is incurred with the presence of metal, using silver should help mitigate these problems. These lasers can also serve as attractive devices to investigate phenomena related to strong light-matter interactions. More importantly, however, they are physically small and easily adaptable to electrical injection, making them attractive candidates for future integration chip-scale onto silicon electronics.

References:

[1] K. Yu, A. Lakhani, and M. C. Wu, "Subwavelength metal-optic semiconductor nanopatch lasers," *Opt. Express*, vol. 18, no. 9, pp. 8790–8799, Apr. 2010.

[2] A. M. Lakhani, K. Yu, and M. C. Wu, "Lasing in subwavelength semiconductor nanopatches," *Semicond. Sci. Technol.*, vol. 26, no. 1, p. 014013, Jan. 2011.

[3] A. M. Lakhani, M. Kim, E. K. Lau, and M. C. Wu, "Plasmonic crystal defect nanolaser," *Opt. Express*, vol. 19, no. 19, pp. 18237–18245, 2011.

[4] M.-K. Kim, A. M. Lakhani, and M. C. Wu, "Efficient waveguide-coupling of metal-clad nanolaser cavities," *Opt. Express*, vol. 19, no. 23, pp. 23504–23512, Nov. 2011.
[5] M.-K. Kim, Z. Li, K. Huang, R. Going, M. C. Wu, and H. Choo, "Engineering of metal-clad optical nanocavity to optimize coupling with integrated waveguides," *Opt. Express*, vol. 21, no. 22, pp. 25796–25804, Nov. 2013.
[6] H. Choo, M.-K. Kim, M. Staffaroni, T. J. Seok, J. Bokor, S. Cabrini, P. J. Schuck, M. C. Wu, and E. Yablonovitch, "Nanofocusing in a metal-insulator-metal gap plasmon waveguide with a three-dimensional linear taper," *Nat. Photonics*, vol. 6, no. 12, pp. 838–844, 2012.